DADLE promotes autophagic flux and depresses necroptosis by inhibiting cytosolic phospholipase A2 mediated lysosomal membrane permeabilization after spinal cord injury

Yituo Chen
Second Affiliated Hospital & Yuying Children's Hospital of Wenzhou Medical University
Haojie Zhang
Second Affiliated Hospital & Yuying Children's Hospital of Wenzhou Medical University
Liting Jiang
Second Affiliated Hospital & Yuying Children's Hospital of Wenzhou Medical University
Wanta Cai
Second Affiliated Hospital & Yuying Children's Hospital of Wenzhou Medical University
Jiaxuan Kuang
Second Affiliated Hospital & Yuying Children's Hospital of Wenzhou Medical University
Yibo Geng
Second Affiliated Hospital & Yuying Children's Hospital of Wenzhou Medical University
Hui Xu
Second Affiliated Hospital & Yuying Children's Hospital of Wenzhou Medical University
Yao Li
Second Affiliated Hospital & Yuying Children's Hospital of Wenzhou Medical University
Liangliang Yang
Wenzhou Medical University
Yuepiao Cai
Wenzhou Medical University
Xiangyang Wang
Second Affiliated Hospital & Yuying Children's Hospital of Wenzhou Medical University
Jian Xiao
Wenzhou Medical University
Wenfei Ni
Second Affiliated Hospital & Yuying Children's Hospital of Wenzhou Medical University
Kailiang Zhou (zhoukailiang@wmu.edu.cn)
Second Affiliated Hospital & Yuying Children's Hospital of Wenzhou Medical University

Research Article

Keywords: DADLE, Autophagic flux, Necroptosis, Cytosolic phospholipase A2, Lysosomal membrane permeabilization, Delta opioid receptor

Posted Date: May 8th, 2023

DOI: https://doi.org/10.21203/rs.3.rs-2886437/v1

Abstract

Programmed cell death plays a critical role in the progression of spinal cord injury (SCI). Autophagy is a protective factor for controlling neuronal damage, while necroptosis promotes further cell death and neuroinflammation after SCI. DADLE (d-Ala2, d-Leu5) is a selective agonist for delta opioid receptor (DOR) and has been identified as a promising drug for its neuroprotective effects. Our present work aims to investigate the therapeutic effect of DADLE on locomotive function recovery following SCI and its concrete mechanism. By establishing a mouse model of spinal cord contusion injury and using functional behavioural assessment, our results showed that DADLE promoted functional recovery after SCI. Through experimental methods such as western blotting and immunofluorescence, we found that DADLE promoted autophagic flux and inhibited necroptosis. Then, analysis of the enzyme activity of NAG and related protein expression of CTSD and CTSB in lysosomes and cytoplasm revealed that DADLE decreased lysosomal membrane permeabilization (LMP). The autophagy inhibitor CQ reversed the protective effect of inhibiting necroptosis. Further analysis identified that DADLE decreased phosphorylated cPLA2, and network pharmacology analysis revealed that the AMPK (Adenosine monophosphate-activated protein kinase) signalling pathway may be involved in the therapeutic effect of DADLE. Finally, blocking the interaction between DOR and DADLE by using naltrindole abolished the anti-phosphorylation effect of DADLE on cPLA2 and p38, resulting in a decrease in autophagic markers and an increase in necroptosis and LMP markers. Altogether, our study indicated that DADLE promotes autophagic flux and inhibits necroptosis by decreasing LMP by interacting with DOR and then activating the AMPK/SIRT1/P38/cPLA2 pathway after SCI, which may have potential clinical application value in the future.

Introduction

Spinal cord injury (SCI) is a serious traumatic organ injury that leads to severe disability and even death. Moreover, patients who suffer from SCI live with a wheelchair and are greatly inconvenienced. According to relevant investigations, the yearly estimated global rate of SCI falls in the range of 250,000 to 500,000 individuals [1, 2]. Mechanically, patients with SCI experience primary injury and secondary injury after impact [3]. Primary injury occurs in a short window of time due to external violence, and secondary injury, which is the most complex and severe phase during SCI, refers to the molecular, chemical, inflammatory cascade and cell death responsible for further spinal cord damage after the first impact [1]. Secondary injury is the most important reason for the deterioration of SCI, and a complete understanding of secondary injury helps us to better understand the pathophysiological process of SCI. Previous studies have indicated that various types of cell death are involved in the pathophysiological process following secondary injury [4–6]. Current evidence has suggestedthat inhibition or promotion of cell death during secondary injury is pivotal to SCI treatment [7, 8].

In the past, apoptosis and necrosis were once believed to be two main types of cell death occurring in organisms [9]. However, different forms of cell death have been discovered in recent years, highlighting that a cell can die by experiencing a number of differing pathways, such as autophagy and necroptosis.

Autophagy is a cellular pathway involved in the degradation of proteins and organelles by the formation of membrane-encapsulated autophagosomes, which are able to fuse with lysosomes and digest their contents [10]. The early stage of autophagy includes the formation of autophagosomes, and the late stage includes the process of fusion between autophagosomes and lysosomes. Both lysosome damage and dysfunctional formation of autophagosomes impair autophagic flux. In previous studies, promoting autophagic flux alleviated motor dysfunction after SCI, so autophagy may be a protective factor against spinal cord injury [11–13]. Necroptosis is a new type of programmed cell death induced by receptor-interacting protein kinase 1 (RIPK1), receptor-interacting protein kinase 3 (RIPK3) and mixed lineage kinase domain-like protein (MLKL) [14]. Necroptosis exacerbates cell death and subsequent neuroinflammation in the pathogenesis of central nervous system (CNS) injury. Moreover, necroptosis mainly occurs in neurons in SCI, inducing early neuronal damage after SCI in adult mice [15, 16]. Therefore, we mainly researched necroptosis in neurons because inhibition of necroptosis in neurons may be of great importance for SCI therapy.

Lysosomes are lipid bilayer membrane-enclosed organelles that mediate the intracellular degradation of macromolecules, and lysosome damage induces an imbalance in cell homeostasis [17]. Thus, maintaining lysosomal integrity and function is of great importance for cellular homeostasis. Lysosomal membrane permeabilization (LMP) is part of lysosomal dysfunction, which causes the leakage of cathepsins and other hydrolases from the lysosomal lumen to the cytosol, resulting in the initiation of various types of programmed cell death [18]. surrounded by a phospholipid-containing membrane, lysosomes are vulnerable to invasion. Many distinct stimuli are able to induce LMP, such as reactive oxygen species, lysosomotropic compounds with detergent activity, and increased concentrations of Ca^{2+}, as well as some endogenous cell death effectors, such as Bax [17]. In addition, phospholipases (PLAs) can easily attack lysosophospholipids, resulting in LMP. There are three major phospholipases A2 (PLAs) found in the CNS: calcium-dependent secretory phospholipase A2 (sPLA2), cytosolic phospholipase A2 (cPLA2), and calcium-independent phospholipase A2 (iPLA2) [19, 20]. Among them, cPLA2 is considered the most important phospholipase because its levels and activity increase in numerous CNS injuries, including SCI [20]. Pharmacological and genetic blockade of cPLA2 has been shown to reduce tissue damage and improve motor functional recovery in SCI. However, drugs that inhibit cPLA2 in SCI are still poorly studied.

The normal functioning of lysosomes affects the balance between autophagy and necroptosis in cells. The late stage of autophagy refers to fusion between autophagosomes and lysosomes, and the permeability of the lysosomal membrane makes it difficult for autophagy to occur. Inhibition of autophagy usually causes induction of necroptosis. A previous study showed that impaired autophagic flux caused by myocardial ischaemic damage activates necroptosis [21]. In addition, necroptosis markers RIPK1 and MLKL were confirmed to be increased in SCI for dysfunctional degradation in lysosomes, and restoration of autophagy-lysosomal function attenuated necroptosis after SCI [16]. These findings led us to speculate that destruction of the lysosome membrane may impair autophagic flux and further cause necroptosis. Normally, increased autophagy attenuates necroptosis, preventing damage and

inflammation caused by necroptosis [8, 22]. This phenomenon indicates that autophagy and necroptosis are in an antagonistic status. Therefore, we can take advantage of autophagy to reduce the neuroinflammation caused by necroptosis.

DADLE is a synthesized opioid peptide that primarily binds to DOR [23]. DOR is a G protein-coupled receptor (GPCR) that is highly expressed in the CNS [24]. Growing evidence has indicated the biochemical benefits and physiological effects of DOR in neuroprotection [25–27]. Previous studies have further shown that DOR signalling triggers different neuroprotective mechanisms, such as ionic homeostasis maintenance, glutamate excitotoxicity alleviation, and Bax-related apoptosis inhibition [28]. Moreover, DADLE was proven to have cytoprotective effects by promoting autophagy, further improving cell survival and exerting neuroprotective effects against ischaemia [28, 29]. DADLE is not only beneficial to the formation of autophagosomes by activating the mTOR signalling pathway but also promotes autophagic flux [29]. However, whether DADLE promotes autophagic flux by preventing lysosome dysfunction remains unknown. In addition, a recent study reported that DOR activation by using TAN-67 led to the prevention of OGD/R-induced injury by inhibiting necroptosis [30]. DADLE also works as a DOR agonist, but few studies have discussed whether DADLE has the potential to inhibit necroptosis to promote neural recovery following SCI. Additionally, DOR activation exerts its neuroprotective effects via a variety of pathways, such as the AMPK signalling pathway, PI3K pathway, and MAPK pathway [23, 27]. However, the therapeutic function of DADLE in SCI has rarely been researched, especially the relationships between DADLE and cell death following SCI. Based on its neuroprotective effect, we selected DADLE as our experimental agent to verify its role and mechanism in SCI recovery.

Materials and methods

Mouse spinal cord injury contusion model

Female animals are commonly used in experimental studies on spinal cord injury (SCI) due to their shorter urethra, which makes artificial voiding to prevent urine retention after SCI easier compared to male animals. [31]. Healthy adult C57BL/6 mice (female, average weight 25–30 g) originated from Wenzhou Medical University's Experimental Animal Center (Licence no. SCXK [ZJ]LY2020-0001), Zhejiang Province, China.

To construct spinal cord contusion model, mice were first anesthetized with 1% sodium pentobarbital (50 mg/kg, i.p.) to induce anesthesia. Then, a standard T9-10 laminectomy was performed to expose the spinal cord by sequentially dissecting the skin and muscles on the back. Subsequently, a Spinal Cord Impactor was used to induce moderate SCI by releasing a 10 g weight bar with 3.0 mm diameter from a height of 20 mm onto the exposed spinal cord surface. After spinal cord injury, the integrity of the spinal cord was carefully observed for any signs of bleeding or rupture. In the end, muscle, fascia, and skin were sutured layer by layer with 4-0 nonabsorbable silk sutures. Mice in the sham group underwent the same operation as mentioned above, without any injury induced by weight drop. Postoperatively, mice were manually assisted with urination three times a day, and were housed under standard conditions including

a temperature of 21-25°C, a 12-hour light/dark cycle, and 50-60% humidity, with free access to water and food. The experimental procedure related to animals followed the Guide for the Care and Use of Laboratory Animals of the China National Institutes of Health, as accepted by the Animal Care and Use Committee of Wenzhou Medical University (wydw 2017-0096).

Antibodies and reagents

Topscience in Shanghai, China, manufactured the DADLE (TP1905) used in this study. Solarbio Science & Technology in Beijing, China, provided the pentobarbital sodium, the Masson staining instrument (Catalogue Number: G1340), the haematoxylin and eosin (HE) staining tools (Catalogue Number: G1120), Nissl staining kit (Catalogue Number: G1430), lysosomal protein extraction kit (Catalogue Number: EX1230) and N-Acetyl-β-D-Glucosidase (NAG) activity assay kit (Catalogue Number: BC4295). Sigma–Aldrich in St. Louis, Missouri, US, supplied chloroquine (CQ, Catalogue Number: C6628), Anti-cPLA2 antibody (SAB4502200) and Anti-Phospho-cPLA2 antibody (Catalogue Number: SAB4503812). Med Chem Express in the United States of America provided dorsomorphin (compound C, Catalogue Number: HY-13418A) and naltrindole hydrochloride (Nal, Catalogue Number: 111469-81-9). Applied Biological Materials in Jiangsu, China, developed the AAV- Pla2g4a Virus (Mouse) (serotype# 1, with no fluorescent reporter gene) and AAV-vehicle Control Virus (serotype# 1, with no fuorescent reporter gene). Cell Signaling Technology in Beverly, Massachusetts, US, provided the primary antibodies against Beclin-1 (Catalogue Number: 3738), LC3B (Catalogue Number: 3868), SIRT1 (Catalogue Number: 9745t), RIP (Catalogue Number: 3493), RIP3 (Catalogue Number: 95702) and cleaved caspase-8 antibodies. The Proteintech Group in Chicago, Illinois, US, produced the CTSD (Catalogue Number: 21327-1) antibodies, GAPDH (Catalogue Number: 10494-1) antibodies the secondary antibodies goat anti-mouse IgG (H+L), HRP conjugate (Proteintech, SA00001-1) and goat anti-rabbit IgG (H+L), HRP conjugate (Proteintech, SA00001-2). Abcam in Cambridge, UK, provided the goat anti-mouse IgG H&L (Alexa Fluor® 594) (Catalogue Number: ab150116), goat anti-mouse IgG H&L (Alexa Fluor® 488) (Catalogue Number: ab150113), goat anti-rabbit IgG H&L (Alexa Fluor® 488) (Catalogue Number: ab150077), goat anti-rabbit IgG H&L (Alexa Fluor® 594) (Catalogue Number: ab150080), microtubule-associated protein-2 (MAP2) (Catalogue Number: ab5392), mouse monoclonal to NeuN (Catalogue Number: ab104224), rabbit monoclonal to NeuN (Catalogue Number: ab177487), p62/SQSTM1 (Catalogue Number: ab240635), CTSB (Catalogue Number: ab214428). Affinity Biosciences in Ohio, US, supplied PI3 Kinase Class III (VPS34, Catalogue Number: DF7921), MLKL (Catalogue Number: AF7919), p38(Catalogue Number: BF8015), p-p38 (Catalogue Number: AF4001) antibodies. The 4’,6-diamidino-2-phenylindole (DAPI) solution was provided by Beyotime Biotechnology in Jiangsu, China.

Adeno-associated virus (AAV) vector packaging

AAV-cPLA2 (mouse Pla2g4e) and AAV-Vehicle (mouse Blank) were constructed and packaged by Applied Biological Materials Company Co., Ltd. (Jiangsu, China). The detailed protocols were conducted according to previously published instructions [32, 33]. The titres of AAV-cPLA2 and AAV-vehicle were

5.63×10^{12} genomic copies and 8.74×10^{12} genomic copies per ml respectively under the analysis of quantitative PCR (qPCR).

Drug and AAV vector administration

We separated 255 mice in a random manner into thirteen groups: Sham (n=25), Sham + AAV-vehicle (n=5), Sham+AAV-cPLA2 (n=5), SCI (n=45), SCI+DA (n=55), SCI+DA+CQ (n=10), SCI+AAV-vehicle (n=15), SCI+AAV-cPLA2 (n=15), SCI+DA+AAV-vehicle (n=15), SCI+DA+AAV-cPLA2 (n=15), SCI+Nal (n=15), SCI+DA+Nal (n=20), SCI+DA+Nal+CQ (n=5), SCI+CC (n=5), SCI+DA+CC (n=5). The DADLE was dissolved in phosphate bufer saline (PBS) and was injected intraperitoneally in DADLE group as previous study recorded (16mg/kg/day) [34]. The CQ was dissolved in DMSO and then diluted in coil oil at concentration of 1%, Comound C and Naltrindole hydrochloride were dissolved in PBS. Daily intraperitoneal injection of CQ (60 mg/kg), Naltrindole hydrochloride(10 mg/kg) and compound C (1.5 mg/kg) was performed 30 min prior to DADLE administration for 3 days. The dose and time of Nal, CC and CQ administration were chosen according to previous studies on CNS trauma [34-36]. The mice were killed by overdosing them with pentobarbital sodium, and processed for western blot at 3 days after injury, and histological samples were acquired for corresponding experiments on days 3 and 28. The SCI + AAV-vehicle control, SCI+AAV-cPLA2, SCI+DA+AAV-vehicle control and SCI+DA+AAV-cPLA2 groups received a 100-μl intravenous injection of the viral vectors in PBS 14 days before SCI. After 14 days, the SCI+DA+AAV-vehicle control and SCI+DA + AAV-cPLA2 groups received the same treatment as the DA group, while SCI + AAV-vehicle control and SCI+AAV-cPLA2 groups only received operation. The animals were killed by overdosing them with pentobarbital sodium, and histological samples were acquired for corresponding experiments on days 3 and 28.

Functional behavioural assessment

BMS scores was utilized to evaluate motor function at 0, 1, 3, 7, 14, and 28 days after spinal cord injury in mice. The BMS score ranges from 0 to 9, with 0 representing complete motor paralysis in mice and 9 representing mice with normal motor function. Footprint analysis was also applied to evaluate motor function at 28 days after surgery. The hind limbs were stained in red and forelimbs in blue using different color dyes. The results were measured by two independent testers who were blinded to the experimental conditions.

Hematoxylin-Eosin Staining, Masson staining and Nissl Staining

On day 28 post-surgery, mice were re-anesthetized using 2% (w/v) pentobarbital sodium and perfused with PBS saline to prepare the spinal cord tissue. Subsequently, the spinal cord tissue containing the lesion (15 mm long, epicenter in the center) was dissected and fixed in 4% (w/v) paraformaldehyde for 48 h. Then, the samples were embedded in paraffin and respective longitudinal and cross sections were prepared. Longitudinal sections of 4 μm thickness were cut using a microtome in preparation for next step. The prepared tissue sections slides are degreased and dehydrated, followed by immersion in Masson staining solution. Subsequently, they are washed multiple times with distilled water, then

dehydrated, and mounted on slides according to established protocols. For HE staining, the tissue sections are degreased and dehydrated, followed by immersion in hematoxylin dye, washing with distilled water, soaking in eosin dye, and washing with distilled water again. Finally, the slides are dehydrated and sealed. The crossed sections of spinal cord from mice at 28 days were incubated in 1 % cresyl violet acetate for Nissl staining. Finally, a light microscope (Olympus, Tokyo, Japan) was used to acquire images. Masson-stained lesion area (blue) was measured by using thresholding method in Image J software. Number of Nissl-stained ventral motor neuron was counted manually in a double-blind manner.

Western blot (WB) analysis

Mice were euthanized on day 3 under SCI, and the spinal cord parts containing lesion part from mice (1.5 cm; covering the injury epicentre) were isolated and stored at -80°C prior to WB. Then RIPA, PMSF and phosphatase inhibitors were added to the tissue in 1.5 ml griding tubes. Ten minutes later, the samples were placed in a homogenizer for the preparation of tissue homogenate. After the supernatant was absorbed, the supernatant was centrifuged for 5 minutes at 3000 rpm. Absorb the supernatant again process with ultrasound for 3 times. The supernatant was sent to the next centrifuge for 5 minutes at 12000 rpm. After centrifugation, the samples made from the supernatant are placed on ice for the next experiment. BCA assays were used for protein quantification. We performed 12% (w/v) gel electrophoresis to separate equal amounts of protein (60 μg); the samples were then transferred to polyvinylidene fluoride membranes (Roche Applied Science, Indianapolis, IN, the United States of America), which were blocked in 5% (w/v) skimmed milk and probed with the following antibodies overnight at 4°C: Beclin1 (1:1,000), SQSTM1/p62 (1:1,000) LC3B (1:1,000), VPS34 (1:1,000), CTSD (1:1,000), CTSB (1:1000), RIPK1 (1:1,000), RIPK3 (1:1,000), MLKL (1:1,000), c-caspase8 (1:1,000), cPLA2 (1:1000), p-cPLA2 (1:1000), p38 (1:1000), p-p38 (1:1000), p-AMPK (1:1,000), AMPK (1:1,000), Sirt1 (1:1000), GAPDH (1:1,000). The membranes were subsequently incubated with HRP-conjugated IgG secondary antibodies at an ambient temperature for 2 h. Using a ChemiDocTM XRS + Imaging System (Bio-Rad) based on an ECL immune-detection tool, band signals were visualized and investigated.

Immunofluorescence (IF) staining

On day 3 after SCI, spinal cord specimens from mice were dissected and collected for IF staining. We performed IF staining on the tissue side according to the rostral spinal cord (1 mm long, 4 mm from the epicentre) following a previous description. We deparaffinized, rehydrated, washed, and then treated the sections with 10.2 mM sodium citrate buffer for 20 min at 95°C. Subsequently, we permeabilized the sections with 0.1% (v/v) PBS-Triton X-100 (10 min). Next, we blocked the sections with 10% (v/v) bovine serum albumin in PBS (1 h). The slides were then incubated overnight at 4°C with antibodies against CTSD (1:200)/NeuN (1:400), LAMP 1 (1:100)/CTSB (1:400), LC3 (1:200)/NeuN (1:400), p62 (1:200)/NeuN (1:400), RIPK1 (1:200)/NeuN (1:400), RIPK3 (1:200)/NeuN (1:400) p-p38 (1:200)/NeuN (1:400) and MAP2 (1:200). Next, we washed the sections for 10 min at an ambient temperature 3 times and incubated them at an ambient temperature for 1 h with FITC-conjugated secondary antibody. Finally, we captured and evaluated images with a fluorescence microscope (Olympus, Tokyo, Japan) within six fields taken in a

random manner in three random sections pertaining to the respective sample. The Immunofluorescence intensity of MAP2, p62, RIPK1, RIPK3, p-cPLA2 and p-p38 in each neuron was estimated by utilizing ImageJ software. IF images of LC3 puncta in each neuron were counting using Image J software. Number of diffused CTSD was estimated manually in a double-blind manner. Number of positive CTSB lysosome in each neuron was estimated manually in a double-blind manner.

Subcellular fractionation and preparation of lysosome protein extraction

4 mm Spinal cord tissue fragments obtained from mice were gathered and homogenized on ice using a Dounce tissue grinder. Purified lysosomal protein components obtained by differential centrifugation of spinal cord homogenate according to protocol of the manufacturer (Lysosomal Protein Extraction Kit; Solarbio Science & Technology). The resulting supernatant fractions were saved as cytosolic fractions. Isolated lysosome protein fractions and cytosolic fractions were stored at -80 °C for further research.

NAG activity assay

NAG was estimated with N-Acetyl-β-D-Glucosidase (NAG) activity assay kit following the manufacturer's instructions. Fluorescence released from the synthetic substrate was measured using a fluorescent plate reader at absorbance of 450 nm for NAG activity. NAG activities in the lysosomal or cytosol fraction were evaluated as change in absorbance per ml of extracting solution.

Collection of targets of SCI and prediction of targets of DADLE

The disease targets of SCI were derived by searching the databases. With the key words including "spinal cord injury", targets related to SCI were founded in the the GeneCards. The target of DADLE was processed from a website (SwissTargetPrediction) using for compound target prediction by giving a canonical SMILE. And the canonical SMILE was download from pubchem. These target genes were took an intersection for subsequent KEGG analysis.

Kyoto encyclopedia of genes and genomes (KEGG) enrichment analyses

The database for annotation, visualization and integrated discovery (metascape, version 3.5.20230101) was used to carry out KEGG enrichment analysis on the intersection target genes. Metascape utilizes the well-adopted hypergeometric test and Benjamini-Hochberg p-value correction algorithm to identify all ontology terms that contain a statistically greater number of genes in common with an input list than expected by chance [37]. KEGG is a knowledge base for systematic analysis of gene functions and related pathway involving in.

Statistical analysis

We completed all statistical investigations using SPSS ver. 19 software (SPSS, Chicago, IL) and adopted a double-blind approach during the analysis process. Values are expressed as the mean ± standard error

of the mean (SEM). To control for unwanted sources of variation, data normalization was performed in this study. Two-way ANOVA followed by Tukey's multiple comparisons test were used to analyse diferences among three or four groups when the data were normally distributed, and nonparametric Mann–Whitney U tests were used for groups if the data were not normally distributed. We employed an independent-sample t-test to compare two independent groups. The p-values less than 0.05 indicated statistical significance.

Results

DADLE promotes mouse locomotive function recovery after SCI

DADLE is a neuroprotective opioid peptide, so we first detected whether it plays a role in functional recovery after SCI. HE, Masson and Nissl staining, IF staining, footprint analysis, and BMS scores were used to evaluate motor function following SCI. HE and Masson results showed that lesions in the spinal cord were obviously smaller with DADLE treatment than in the SCI group (**Fig. 1A-B**). Spinal cord specimens exhibited the same result (**Fig. 1G**). Additionally, Nissl staining and IF staining revealed that anterior horn neurons and neural MAP 2 expression in the SCI group were lower in the DADLE treatment group than in the sham group (**Fig. 1C-F**). Furthermore, we evaluated motor function by analysing BMS and footprint analysis. The sham group showed a normal BMS sore and footprint (**Fig. 1H-I**). In the SCI group, the BMS scores at 3, 7, 14, 21 and 28 days were obviously lower than those in the sham group, while the DADLE treatment group achieved significantly greater scores than the SCI group at 14, 21 and 28 days. Likewise, footprint analysis of the SCI group exhibited a shorter step distance of the posterior limb; however, DADLE treatment significantly reversed the reduced step distance (**Fig. 1H-I**). All these results indicated that DADLE is able to promote functional recovery after SCI.

DADLE promotes autophagic flux in SCI

As a major way to eliminate harmful components, autophagy is extremely crucial in neurons, which are terminally differentiated cells that must last the lifetime of the organism [38]. Impairment of autophagic flux in SCI is strongly related to neuronal death and recovery of motor function [39]. Thus, reducing neuronal death is important for the recovery of motor function after SCI. Promoting autophagy in motor neurons contributes to motor function recovery, indicating that autophagy is a neuroprotective factor for SCI [40]. To further ascertain the role of autophagy in SCI after treatment with DADLE, we detected autophagy-related indicators. The class III PI-3 kinases, notably VPS34 (vesicular protein sorting 34) and its binding partner Atg6/Beclin-1, are collectively involved in phagophore formation [41]. LC3B-II, which is processed by LC3B (microtubule-associated protein light chain 3) through various reactions, is a great marker of autophagosomes [41]. p62/SQSTM1 is an autophagic substrate protein, and accumulation of p62 indicates inhibition of autophagic flux. Therefore, we detected the protein expression levels of VPS34, beclin-1, LC3B and P62. As shown in **Fig. 2A and B**, we observed a significant increase in the protein expression of autophagy indicators such as VPS34, Beclin-1 and LC3 in the DADLE

treatment group compared with the SCI group. IF staining showed fluorescence images of p62 and LC3 in neurons, which showed that the fluorescence intensity levels of p62 were higher than those in the sham and SCI+DA groups, while the number of LC3 fluorescence puncta in neurons of the SCI+DA group was greater than that in the sham and SCI groups (**Fig. 2C-F**). These results revealed that DADLE may promote autophagy in the initial phase. However, an increase in LC3 may be attributed to the blockage of fusion with autophagosomes and lysosomes or an increase in the formation of autophagosomes [42]. p62 increased in the SCI group compared to the sham group, while adding DADLE obviously decreased p62 expression after SCI (**Fig. 1A-B**). To confirm whether DADLE promotes autophagic flux, we estimated LC3 expression by the addition of CQ, which can block the interaction between lysosomes and autophagosomes. The results showed that LC3 II levels in the SCI and SCI+CQ groups were not significantly different, while the SCI+DA and SCI+DA+CQ groups exhibited significant differences (**Fig. 2 G-H**). Undoubtedly, autophagic flux is blocked after SCI, but DADLE treatment contributes to the recovery of autophagic flux. These data indicated that DADLE promotes autophagic flux.

DADLE inhibits necroptosis after SCI

MLKL aggregates on the cell membrane in necroptosis, inducing neural rupture and death, leading to neuroinflammation and impaired motor function[15, 43]. As neuronal necroptosis may be a key factor in neurodegenerative disorders, inhibiting necroptosis appears to give rise to neuroprotective effects by rescuing neurons [43]. Therefore, decreasing necroptosis in neural cells may contribute to motor function recovery. We next used WB analysis and IF staining to detect the necroptotic indicators RIPK1, RIPK3, MLKL and cleaved caspase-8. WB results showed that the protein expression of RIPK1, RIPK3, MLKL and cleaved caspase-8 increased in the SCI group compared to the sham group, which indicated the occurrence of necroptosis in SCI (**Fig. 3A-B**). However, the protein expression levels of RIPK1, RIPK3 and MLKL decreased, while the levels of cleaved caspase-8 increased significantly in the SCI+DA group compared to the SCI group, indicating inhibition of necroptosis (**Fig. 3A-B**). IF staining reflected the fluorescence intensities of RIPK1 and RIPK3 in neural cells. Similarly, in comparison to the SCI group, the fluorescence intensity of RIPK1 and RIPK3 in neurons was lower in the SCI+DA group (**Fig. 3C-F**). Altogether, these results showed that the restorative effect of DADLE after SCI was partly due to the suppression of necroptosis.

DADLE inhibits lysosomal membrane permeabilization after SCI

As described previously, autophagic flux is blocked after SCI, and DADLE can promote recovery of autophagic flux. Lysosome dysfunction causes abnormal infusion of lysosomes and autophagosomes within autophagy, inducing blockade of autophagic flux [18]. LMP is one type of lysosome dysfunction that causes the release of cathepsins and other hydrolases into the cytosol, resulting in the initiation of various types of programmed cell death. In previous studies, LMP occurred in SCI and caused the accumulation of necroptosis-related proteins [16, 20]. Therefore, we hypothesized that DADLE promotes autophagic flux by inhibiting LMP. We detected the protein expression of cathepsin

D (CTSD) and cathepsin B (CTSB) in the cytoplasm and lysosomes. WB results showed higher protein expression of CTSD and CTSB in the cytoplasm and lower expression in lysosomes after SCI compared to the sham group, while the DADLE treatment group reversed these changes (**Fig. 4A-B**). The presence of lysosomal enzymes in the neural cytosol was confirmed by IF staining. In **Fig. 4C**, IF staining of neural CTSD exhibited granular fluorescence in the sham group, but fluorescence was diffuse in the cytoplasm in the SCI group, which indicated that the neural lysosome membrane was damaged and leakage of lysosomal enzymes occurred in SCI. Additionally, overlapping fluorescent puncta of LAMP1 (lysosome associated membrane protein 1) and CTSB in neurons were detected, and the results showed that in the sham group, there were more CTSB-positive lysosomes than in the SCI group, indicating that CTSB diffused in neurons following SCI (**Fig. 4D**). The leakage of lysosomal enzymes into the cytosol indicated that LMP occurs in the spinal cord after SCI. After DADLE treatment, IF staining showed fewer diffuse CTSD neurons and more CTSB-positive lysosomes in each neuron than in the SCI group, indicating a decrease in lysosome destruction (**Fig. 4C-F**). To further examine the effect of DADLE on lysosomal function, we measured lysosomal NAG activity in sham, SCI and DADLE-treated mouse spinal cords with or without SCI contusion after 3 days. The activity of NAG in the cytoplasm was increased in the SCI group compared to the DADLE treatment group **(Fig. 4G**).
However, subcellular fractionation of spinal cord tissues exhibited lower NAG activity in the lysosomal fractions prepared from injured mice compared to the DADLE treatment group. Therefore, the promotion of autophagic flux after SCI is likely due to the decrease in LMP.

Blockage of autophagic flux by CQ weakens the inhibitory effect of DADLE on necroptosis in SCI

We then explored the relationships between necroptosis and autophagy in SCI, so we intended to inhibit autophagy to further detect changes in necroptosis. CQ is a widely used autophagy inhibitor that mainly inhibits autophagy by impairing autophagosome fusion with lysosomes [44]. Our previous work revealed that DADLE may promote autophagic flux by inhibiting LMP (**Fig. 4**). Thus, we used CQ to intentionally inhibit autophagic flux in the same manner as LMP. As shown in **Fig. 5A-B**, the addition of CQ obviously increased the protein levels of necroptosis markers such as RIPK1, RIPK3 and MLKL and decreased cleaved caspase-8 after treatment with DADLE. IF staining of RIPK1 and RIPK3 fluorescence intensity in neurons showed the same results as WB analysis (**Fig. 5C-F**). Our experiment indicated that autophagy antagonizes necroptosis, and inhibition of autophagy promotes necroptosis to further aggravate SCI.

DADLE inhibits LMP by decreasing cPLA2 phosphorylation following SCI

Given that autophagy participates in de novo membrane production and vesicle fusion, extensive changes in lipid molecules are necessary. The lysosomal membrane, which is vulnerable to a variety of substances, prevents lysosomal enzymes from directly destroying neural cells. cPLA2 is able to significantly change the lipid composition of the lysosomal membrane and leads to lysosomal membrane damage [45]. In addition, a previous study reported that phosphorylated cPLA2 is activated and present at lysosomes, inducing lysosomal membrane destruction and blocking autophagic flux [20].

Therefore, we hypothesized that DADLE may decrease LMP by inhibiting the phosphorylation of cPLA2 in neurons. Quantitative WB analysis demonstrated that the ratio of phosphorylated cPLA2 was significantly increased specifically after SCI compared with that in the sham group, and DADLE treatment obviously decreased the phosphorylation of cPLA2 after SCI (**Fig. 6A-B**). Moreover, this result is also supported by IF analysis, where we observed that IF densities of phospho-cPLA2 in each neuron were stronger in the SCI group than in the sham and DADLE groups **(Fig. 6C and Fig6.F**).

To further identify the role of cPLA2 in SCI after DADLE treatment, we designed a rescue experiment by overexpressing cPLA2. First, we compared the protein expression of cPLA2 and p-cPLA2 within the Sham, Sham+AAV-vehicle and Sham+AAV-cPLA2 groups, and the results showed that AAV-cPLA2 obviously increased cPLA2 and p-cPLA2 expression, whereas protein expression between the sham and Sham+AAV-vehicle groups was not statistically significant, indicating that the adenovirus with cPLA2 packaging was effective in overexpressing cPLA2 (**Fig. 6 D-E**). Then, we detected whether cPLA2 expression had an effect on lysosomes after SCI following DADLE treatment. Western blotting analysis demonstrated that AAV-cPLA2 injection further decreased the levels of CTSB and CTSD proteins in lysosomes but increased the levels in the cytoplasm after DADLE treatment (**Fig. S1 A-B**). Simultaneously, co-IF staining of CTSD&NeuN and CTSB&LAMP1 showed more diffuse CTSD neurons in the spinal cord and fewer CTSB-positive lysosomes in each neuron after AAV- cPLA2 administration in the SCI+DA+AAV-cPLA2 groups compared to the SCI+DA+AAV-vehicle groups (**Fig. 6 G-H** and **Fig S1D-E**). The NAG assay results showed that the NAG activity in the cytoplasm significantly decreased after DADLE and blank viral treatment in SCI, while the NAG activity in the lysosome increased. However, the inhibitory effect of DADLE on NAG leakage was reversed by overexpression of cPLA2 (**Fig. S1 C**). This evidence demonstrated that overexpressed cPLA2 reversed the positive function of DADLE in inhibiting LMP. To further determined the relationship between cPLA2, autophagy and necroptosis in SCI, we carried out a rescue experiment with the SCI+AAV-vehicle group, SCI+AAV-cPLA2 group, SCI+DA+AAV-vehicle group and SCI+DA+AAV-cPLA2 group. As shown in **Fig S2G-H**, WB analysis revealed increased necroptosis and autophagic substrate markers after administration of AAV-cPLA2 in the SCI+AAV-cPLA2 group and SCI+DA+AAV-cPLA2 group. Additionally, the increase between the SCI+DA+AAV-cPLA2 group and DA+AAV-vehicle group was significantly higher than that between the SCI+AAV-cPLA2 group and SCI+AAV-vehicle group (**Fig-S2 G-H**). IF staining showed the fluorescence intensity of RIPK1, RIPK3, P62, and LC3 in the neurons of groups SCI+AAV-vehicle, SCI+AAV-cPLA2, SCI+DA+AAV-vehicle, and SCI+DA+AAV- cPLA2, respectively (**Fig S2A-F**). Compared with the SCI+AAV vehicle group, the fluorescence intensity of RIPK1 and RIPK3 in neurons was significantly reduced after the addition of DADLE (**Fig S2A-C**). However, the inhibition of necroptosis by DADLE was reversed by overexpression of cPLA2 (**Fig S2A-C**). In comparison of the SCI+DA+AAV-vehicle group and the SCI+DA+AAV-cPLA2 group, the fluorescence intensity of the autophagy substrate p62 and the fluorescence puncta number of the autophagy marker LC3 in neural cells significantly increased after cPLA2 overexpression (**Fig S2D-F**). However, there was no significant difference in the fluorescence puncta number of LC3 between the SCI+AAV-vehicle group and the SCI+AAV-cPLA2 group (**Fig S2D-F**). These results were consistent with the

WB analysis. In addition, these data were similar to our previous work that blockade of lysosome by administration of CQ after DADLE treatment inhibited autophagic flux and promoted necroptosis (**Fig. 2 G-H** and **Fig. 5**). All of these results suggested that DADLE treatment may inhibit the activation and presentation of cPLA2 on lysosomes, further decreasing LMP and subsequently blocking autophagic flux after SCI.

DADLE promotes autophagy and inhibits necroptosis through the DOR-AMPK-SIRT1-P38 pathway in SCI

To confirm which pathway is involved in the neural protective function of DADLE, we searched for downstream targets of DADLE and SCI genes from SwissTargetPrediction and GeneCards. We took the intersection of the results, and Vein gram indicated that 88 genes may have to do with the therapeutic role of DADLE in SCI (**Fig. 7A**). Next, we selected 88 genes for KEGG analysis, and the results showed that the top 20 pathways participated in DADLE treatment, such as the AMPK signalling pathway, cAMP signalling pathway and phospholipase D signalling pathway (**Fig. 7B**). Activation of the AMPK signalling pathway has been proven to be beneficial to functional recovery after SCI in previous studies, and activating the AMPK signalling pathway promotes autophagy [46-49]. Thus, we selected the AMPK signalling pathway for subsequent research. Simultaneously, cPLA2 can be phosphorylated by MAPK (mitogen-activated protein kinases) to interact with downstream molecules, and p38 was identified to be inhibited after DADLE treatment, so we also detected MAPK p38 [50-52]. WB results showed that p-AMPK and SIRT1 (sirtuin 1) were decreased but p-p38 was increased in the SCI group compared with the sham group (**Fig. 7E-F**). However, these effects were reversed by DADLE treatment (**Fig. 7E-F**). **Fig. 7C** showed IF staining image of p-p38 in neurons, and results showed IF densities of p-p38were lower in the sham group and DADLE treatment group than in the SCI group (**Fig. 7C-D**). Therefore, we assumed that DADLE may inhibit cPLA2 through the AMPK/SIRT1/P38 pathway. To further prove the AMPK/SIRT1/p38 pathway in SCI, we used the AMPK inhibitor Compound C to inhibit the AMPK pathway, and WB analysis revealed that AMPK, p-AMPK and SIRT1 were reduced while p-p38 was increased in the SCI+CC group compared with the SCI+DA group (**Fig. 7G-H**). Therefore, the AMPK/SIRT1/p38 pathway is involved in DADLE treatment in SCI.

By consulting previous literature, we can learn that DADLE gives play to its neuroprotection effect by combining with delta opioid receptor. Thus, we decided to verify whether DOR participates in the upstream of AMPK signal pathway. We added DOR inhibitor naltrindole to block the interaction between DADLE and DOR. From the analysis of WB results, the addition of naltrindole in the SCI group did not affect the expression of p-AMPK, SIRT1, or p-p38, while the addition of naltrindole in the DADLE treatment group significantly inhibited the expression of p-AMPK, SIRT, but increased the expression of p-p38 and p-cPLA2 (**Fig. 8A-B**). Simultaneously, protein expression of necroptosis markers was increased after treatment with naltrindole compared with SCI+DA group. In addition to that, autophagy marker LC3 II was decreased and autophagy substrate p62 was increased after adding naltrindole in the SCI+DA+Nal group compared with the SCI+DA group, but showed no significance between SCI and SCI+Nal group (**Fig. 8C-D**). These results may be attributed to little DOR activation after SCI, but artificial injection of DADLE activated DOR, which promoted the occurrence of autophagy and the inhibition of necroptosis, and this

effect could be inhibited by naltrindole. Next, we detected autophagy flux by injection of CQ, and the increase of related protein expression of LC3 II between the SCI+DA and SCI+DA+CQ group was significantly greater than that between the SCI+DA+Nal and SCI+DA + Nal + CQ group, so as to p62 (**Fig. 8E-F**). Thus, administration of naltrindole in DADLE treatment group will impair DADLE function to restore autophagic flux following SCI. Altogether, these results showed that DADLE inhibits phosphorylation of cPLA2 by activating DOR/AMPK/SIRT1/p38 pathway, and inhibition of AMPK signalling pathway by blocking the interaction with DOR causes blockage of autophagic flux and promotion of necroptosis.

Inhibition of DOR-AMPK-SIRT1-P38 pathway reverses neural protective effect by DADLE after SCI

Next, we conducted another behavioural experiment after adding naltrindole. The HE and Masson results showed that lesions in the spinal cord were larger in the SCI+DA + Nal group than in the DADLE group, while in the SCI and SCI + Nal groups, there was no difference (**Fig S3A-B**). Spinal cord specimens exhibited the same result (**Fig S3C**). In addition, Nissl staining revealed that anterior horn neurons were reduced after treatment with naltrindole in the DADLE treatment group (**Fig S3D-E**). IF staining indicated that neural MAP2 fluorescence intensities in the SCI+DA+Nal group were obviously lower than those in the DADLE group, while no significant difference was found in the SCI and SCI+Nal groups **(Fig S3F-G)**. We also evaluated motor function by analysing BMS and footprint analysis, and the results showed that the BMS score at 3, 7, 14, 21 and 28 days and the distance of the step of the posterior limb at 28 days exhibited no significant difference between the SCI and SCI + Nal groups but were obviously lower in the SCI+ DA + Nal group than in the DADLE group (**Fig S3H-I**). These outcomes may be due to the lack of significant activation of DOR after SCI, while injection of DADLE to activate DOR caused a series of reactions to promote injury recovery. Altogether, these results indicated that DADLE is capable of promoting functional recovery after SCI through interaction with DOR.

Discussion

According to the pathological process, traumatic SCI is divided into two stages: primary injury and secondary injury. With a large number of studies focused on secondary injury, it is normally thought that the progression of SCI may be attributed to cell death and neuroinflammation. Cell death inevitably occurs in SCI and causes motor dysfunction. Thus, inhibition of cell death may contribute to functional recovery after SCI. DADLE is a synthetic opioid peptide that functions by interacting with DOR. In the past, researchers have studied the pharmacological function of DADLE in brain ischaemia–reperfusion injury, oxygen-glucose deprivation (OGD) and spinal cord ischaemia and reperfusion injury [51, 53]. This evidence indicates that DOR activation by DADLE may exert a neuroprotective role after neural injury. However, few studies have researched the protective role of DADLE in traumatic SCI and its concrete mechanism. Our present study provides novel evidence indicating that DADLE plays an important role in inhibiting necroptosis and promoting autophagic flux following SCI by inhibiting LMP through the DOR/AMPK/SIRT1/p38/cPLA2 pathway. Through BMS score and footprint analysis, we found that the administration of DADLE to mice significantly restored motor function in comparison with the SCI group. Additionally, DOR activation promotes autophagic flux and inhibits necroptosis by decreasing the

destruction of the lysosome membrane attacked by p-cPLA2. Notably, inhibition of the AMPK-SIRT1-P38 pathway by blocking the interaction of DOR will reverse the neuroprotective function of DADLE. Thus, DADLE can be used as a potential drug for treating SCI in the future.

Autophagy, a lysosome-based degradation process, is evolutionarily conserved and plays a critical role in diverse pathophysiological conditions across various environments. [54]. There are two steps of autophagy: a. formation of autophagosome and b. autophagosome fusion with the lysosome to become an autolysosome, which is able to degrade the components contained within it. In the initiation phase of autophagy, induction, nucleation and elongation of autophagosome formation requires a variety of complexes, such as the ATG family, VPS34 and beclin-1 [55]. As previous studies have shown, autophagy has been identified as a therapeutic intervention target for SCI, and autophagy may protect and promote neuronal recovery after SCI [54, 56]. DADLE promotes autophagy by augmenting autophagosomes to improve neuronal survival and exert neuroprotective effects against ischaemia [29]. In our work, we found that DADLE increased the expression of VPS34, beclin-1 and LC3 compared with that in the SCI groups, indicating the promotion of autophagy initiation. The autophagic substrate p62 accumulated after SCI, which was relieved by administration of DADLE. This phenomenon indicated that autophagic flux may be promoted after DADLE treatment. To further detect whether an increase in LC3 II augments autophagosome synthesis or inhibits fusion between autophagosomes and lysosomes, we used the lysosome inhibitor CQ to assess autophagic flux. Furthermore, we found that DADLE treatment aggravated the accumulation of LC3 II and the autophagic substrate p62 after adding CQ, indicating that DADLE treatment fixes the impairment of autophagic flux. Previous studies have reported that impairment of autophagy occurs in SCI due to lysosomal dysfunction. Therefore, we speculated that DADLE promotes the recovery of autophagic flux by regulating lysosome function.

Necroptosis is a regulated form of necrosis mediated by RIPK1 and RIPK3 that is capable of exacerbating cell death and neuroinflammation in the pathogenesis of central nervous system (CNS) diseases [16, 57]. Activation of RIPK1 triggers necroptosis by forming a complex with RIPK3 and MLKL, wherein RIPK3 phosphorylates MLKL, causing cellular membrane disruption and subsequent cell lysis [58]. Inhibition of necroptosis promotes functional recovery after SCI [59, 60]. Therefore, we hypothesize that DADLE may inhibit necroptosis to exert neuroprotective effects. In this study, we found decreased expression of necroptosis marker proteins such as RIPK1, RIPK3 and MLKL and increased caspase-8 by using WB analysis and IF staining in the DADLE groups, indicating that DADLE inhibits necroptosis. Furthermore, we attempted to elucidate the relationships between autophagy and necroptosis after DADLE treatment following SCI. In previous studies performed by our team, inhibition of autophagy aggravated necroptosis after SCI [22, 35]. Similarly, we also obtained the same result: blockade of autophagic flux by CQ reversed necroptosis inhibition after DADLE treatment. This result revealed that autophagy and necroptosis are antagonistic to each other, and inhibition of autophagy will facilitate the further development of necroptosis. Autophagy is a self-degradative process that can eliminate harmful substances, and augmenting autophagy may eliminate necroptotic markers such as RIPK1, RIPK3 and MLKL, thus inhibiting necroptosis. However, the specific connection and biochemical mechanism need to be further

studied. Altogether, these results demonstrated that DADLE inhibited necroptosis via autophagy enhancement, which plays a critical role in motor function recovery after SCI.

Lysosomes serve as cellular recycling centres for cargo received mainly through autophagy and endocytosis [61]. The lysosomal membrane is vulnerable to different forms of stress, and any substance that can destroy the lysosomal membrane will cause LMP. Lysosome membrane destruction induces leakage of intralysosomal components out of lysosomes, which further causes programmed cell death [18]. However, LMP blocks the fusion of autophagosomes and lysosomes, resulting in inhibition of autophagic flux. Here, we hypothesized that LMP plays an important role in lysosomal dysfunction in SCI. In our present work, by isolating lysosomes from the cytoplasm and analysing the distribution of NAG, CTSB and CTSD, we found that the protein expression of CTSB and CTSD and the enzyme activity of NAG increased in the cytoplasm but decreased in lysosomes after SCI. IF staining also showed more diffuse CTSD neurons and fewer CTSB-positive lysosomes in each neuron in the SCI group than in the sham group. These results indicate that components in lysosomes flowed out of lysosomes, which may account for the destruction of the lysosome membrane. After DADLE treatment, lysosome enzymes such as CTSD, CTSB and NAG decreased in the cytoplasm and increased in lysosomes. IF staining also revealed a decrease in diffuse CTSD neurons and CTSB-positive lysosomes in each neuron after DADLE treatment following SCI, proving that DADLE decreased LMP and the subsequent leakage of lysosomal contents. Next, we further detected which factor gave rise to LMP. After reviewing previous literature, we found that cPLA2 may be related to SCI, so we designed a series of experiments to verify the relationship between DADLE and cPLA2 [20]. IF staining and WB analysis results showed that DADLE decreased the phosphorylation of cPLA2 after SCI, suggesting that DADLE may inhibit LMP by decreasing phosphorylated cPLA2. Moreover, overexpression of cPLA2 impaired the capability of inhibiting LMP following DADLE treatment, resulting in inhibition of autophagy and promotion of necroptosis. Thus, phosphorylated cPLA2 caused LMP and induced leakage of lysosomal contents, which led to impairment of autophagic flux and aggravation of necroptosis after SCI, and this effect was prevented by DADLE administration. Taken together, these results demonstrated that the therapeutic effect of DADLE was regulated by inhibiting the phosphorylation of cPLA2 to maintain the integrity of the lysosomal membrane.

Next, we investigated which signalling pathway regulates cPLA2 after treating DADLE by using network pharmacology analysis. By collecting SCI-related genes from Genecard and DADLE downstream targets from SwissTargetPrediction, we found that 88 genes may be involved in DADLE treatment in SCI. After KEGG analysis of 88 genes, we found that the cAMP signalling pathway, AMPK signalling pathway and phospholipase D signalling pathway may be involved. AMPK, which is capable of responding to a low-energy state and starvation, can be activated by the ratio of AMP/ATP [62]. Activation of the AMPK signalling pathway contributes to autophagy, and a previous study also proved that DADLE is able to activate AMPK and its downstream signalling molecules [29, 63, 64]. In addition, cPLA2 is phosphorylated by MAP kinase to further activate downstream cascade reactions, and DADLE is reported to inhibit p38 MAPK in different diseases [50–52, 65]. Therefore, we decided to explore whether DADLE regulates cPLA2 by the AMPK signalling pathway and p38 MAPK. WB results showed an increase in the

protein expression of p-AMPK, SIRT1 and p38 after DADLE treatment following SCI. Next, we designed a rescue experiment to further clarify the results. With the use of Compound C, suppressing AMPK after DADLE treatment could reduce the expression of SIRT1 and increase the expression of p-p38 and p-cPLA2, indicating that the AMPK-SIRT1-p38 pathway is activated after DADLE administration in SCI. DADLE functions by interacting with the delta opioid receptor [23, 25]. Thus, we added naltrindole to block the interaction between DADLE and DOR, and the results showed that the influence exerted by DADLE on autophagy and necroptosis was reduced. In addition, the application of naltrindole inhibited the AMPK signalling pathway after DADLE treatment. These results suggest that the effect of DADLE on autophagy and necroptosis is regulated by the DOR-AMPK-SIRT1-p38 pathway.

As a kind of opioid receptor agonist, DADLE also has the ability to ease pain. Given that patients suffering from SCI endure intense pain, DADLE has the potential to relieve pain, which is a very advantageous point for clinical patients. Therefore, future research concerning DADLE needs to combine the analgesic effects with the function of promoting neural function recovery. The advantages of DADLE suggest that it has much promise for use in clinical settings. However, our research also has some limitations requiring in-depth analyses. We described that DADLE triggers the AMPK signalling pathway by interacting with DOR but failed to explore how DOR activates AMPK. In addition to the AMPK signalling pathway, network pharmacology analysis showed that several signalling pathways were also involved in the pharmacological impact of DADLE on SCI, such as the phospholipase D signalling pathway. PLD1 (phospholipase D1) refers to a lipid-hydrolysing enzyme previously implicated in intracellular signalling and vesicle trafficking, which is of vital importance in later stages of autophagy, and inhibition of PLD1 causes blockage of autophagy flux [66]. This is similar to our current research, and future studies can further detect their relationships. While our study demonstrated the involvement of DADLE in the later stages of autophagy, specifically the fusion between autophagosomes and lysosomes, it does not preclude the possibility that DADLE also plays a role in the early stages of autophagy. In our experiment, DADLE treatment contributed to VPS34, beclin-1 and LC3 expression, indicating an increase in autophagosomes. In addition, other studies have reported that DADLE is capable of regulating mTOR, which is a classic autophagy signalling molecule [29, 63]. Moreover, as a G-protein coupled receptor, there may be many connections between DOR and other signalling pathways, which need to be further explored. In addition, our present work on cPLA2 mainly focuses on its influence on the lysosome membrane, but cPLA2 can also function as a message molecule to mediate other signal transduction pathways. Active p-cPLA2 is able to release AA (arachidonic acid) from phospholipids, which is a substrate of COX-2 and mediates the COX-2 signalling pathway [67]. A study reported that abnormal regulation of cPLA2 and the COX-2 signalling pathway leads to hyperexcitability of cortical pyramidal neurons in a mouse model of autosomal-dominant lateral temporal epilepsy [68]. It has also been reported that cPLA2 activation promotes lipid metabolism reprogramming that produces superfluous ROS (reactive oxygen species) to further exacerbate cerebral injury, while inhibition of cPLA2 facilitates neuroprotection after brain I/R injury [69, 70]. After treatment with DADLE, whether cPLA2 participates in other mechanisms to promote the recovery of motor function after spinal cord injury needs further study.

Altogether, we present a neuroprotective drug, DADLE, that maintains the integrity of the lysosome membrane during SCI by reducing phosphorylated cPLA2. We revealed that neuronal autophagy was increased and necroptosis was decreased in an AMPK-dependent manner under in vitro SCI after DADLE treatment, and inhibition of the AMPK-SIRT1-p38-cPLA2 pathway by blocking the interaction between DOR and DADLE aggravated the neurological deficits in SCI models. Therefore, DADLE might be a potential therapeutic drug for future SCI treatment.

Conclusion

After interacting with DOR, DADLE inhibits p38 phosphorylation by activating the AMPK/SIRT1 pathway, which further decreases the phosphorylation of cPLA2. These events lead to inhibition of necroptosis and promotion of autophagic flux by decreasing destruction of the lysosome membrane following SCI (Fig. 8G). Furthermore, DADLE can effectively promote motor functional recovery after SCI, indicating that DADLE takes great advantage of SCI treatment. Thus, our present study suggests that DADLE may work as a promising therapeutic drug for SCI treatment in the future.

Abbreviations

AMPK = Adenosine monophosphate-activated protein kinase

CC = compound C

CNS = central nervous system

cPLA2 = cytosolic phospholipase A2

CQ = chloroquine

CTSB = cathepsin B

CTSD = cathepsin D

DADLE = d-Ala2, d-Leu5

DOR= delta opioid receptor

LAMP 1= lysosome associated membrane protein 1

LC3 II = microtubule-associated protein light chain 3

LMP = lysosomal membrane permeabilization

MAPK = mitogen-activated protein kinases

MLKL = mixed lineage kinase domain-like protein

NAG = N-Acetyl-β-D-Glucosidase

RIPK1= receptor-interacting protein kinase 1

RIPK3 = receptor-interacting protein kinase 3

SCI = spinal cord injury

SIRT1 = sirtuin 1

VPS 34 = vesicular protein sorting 34

Declarations

Acknowledgements

Not applicable.

Author contributions

Yituo Chen and Haojie Zhang drafted and finished experiment plans and manuscript. Liting Jiang and Wanta Cai accomplished the data processing and revise the manuscript. Jiaxuan Kuang, Yibo Geng and Hui Xu assisted in making provision for experiment materials. Yao Li and Liangliang Yang prepared figure 1-8 and figure S1-3.Yuepiao Cai and Xiangyang Wang helps to polish the manuscript. Jian Xiao, Kailiang Zhou and Wenfei Ni checked the revised manuscript. Yituo Chen and Haojie Zhang have contributed equally to this work. All authors have read and approved the final manuscript.

Funding

This work was funded by grants from National Natural Science Foundation of China (No. 82072192 to Kailiang Zhou); Wenzhou Science and Technology Bureau Foundation (No. Y20210438 to Kailiang Zhou); Public Welfare Technology Application Research Project of Zhejiang Province (LGF20H150003 to Kailiang Zhou); Zhejiang Provincial Natural Science Foundation (No. LY21H060009 to Wenfei Ni).

Availability of data and materials

Data and materials are available under reasonable request.

Ethics approval and consent to participate

All animal experiments in this study were conducted in accordance with the Guide for the Care and Use of Laboratory Animals of the China National Institutes of Health. The animal experiments were approved by the Animal Research Committee

Competing interests

All authors report that there are no conflicts of interest related to the present article

Consent for publication

Not applicable.

References

1. Anjum AA-O, Yazid MA-O, Fauzi Daud MA-O, Idris J, Ng AMH, Selvi Naicker A, et al. Spinal Cord Injury: Pathophysiology, Multimolecular Interactions, and Underlying Recovery Mechanisms. LID - 10.3390/ijms21207533 [doi] LID - 7533. (1422-0067 (Electronic)).
2. Khorasanizadeh M, Yousefifard M, Eskian M, Lu Y, Chalangari M, Harrop JS, et al. Neurological recovery following traumatic spinal cord injury: a systematic review and meta-analysis. (1547-5646 (Electronic)).
3. McDonald JW, Sadowsky C. Spinal-cord injury. (0140-6736 (Print)).
4. Shi ZA-O, Yuan S, Shi L, Li J, Ning G, Kong X, et al. Programmed cell death in spinal cord injury pathogenesis and therapy. (1365-2184 (Electronic)).
5. Liu Z, Yao X, Jiang W, Li W, Zhu S, Liao C, et al. Advanced oxidation protein products induce microglia-mediated neuroinflammation via MAPKs-NF-κB signaling pathway and pyroptosis after secondary spinal cord injury. (1742-2094 (Electronic)).
6. Hu X, Chen H, Xu H, Wu Y, Wu C, Jia C, et al. Role of Pyroptosis in Traumatic Brain and Spinal Cord Injuries. (1449-2288 (Electronic)).
7. Abbaszadeh F, Fakhri S, Khan H. Targeting apoptosis and autophagy following spinal cord injury: Therapeutic approaches to polyphenols and candidate phytochemicals. (1096-1186 (Electronic)).
8. Zhou K, Zheng Z, Li Y, Han W, Zhang J, Mao Y, et al. TFE3, a potential therapeutic target for Spinal Cord Injury via augmenting autophagy flux and alleviating ER stress. (1838-7640 (Electronic)).
9. D'Arcy MS. Cell death: a review of the major forms of apoptosis, necrosis and autophagy. Cell biology international. 2019;43(6):582-92.https://doi.org/10.1002/cbin.11137
10. Mizushima N, Levine B, Cuervo AM, Klionsky DJ. Autophagy fights disease through cellular self-digestion. Nature. 2008;451(7182):1069-75.https://doi.org/10.1038/nature06639
11. Zhou K, Zheng Z, Li Y, Han W, Zhang J, Mao Y, et al. TFE3, a potential therapeutic target for Spinal Cord Injury via augmenting autophagy flux and alleviating ER stress. Theranostics. 2020;10(20):9280-302.https://doi.org/10.7150/thno.46566
12. Zhang B, Lin F, Dong J, Liu J, Ding Z, Xu J. Peripheral Macrophage-derived Exosomes promote repair after Spinal Cord Injury by inducing Local Anti-inflammatory type Microglial Polarization via Increasing Autophagy. International journal of biological sciences. 2021;17(5):1339-52.https://doi.org/10.7150/ijbs.54302
13. Wu YQ, Xiong J, He ZL, Yuan Y, Wang BN, Xu JY, et al. Metformin promotes microglial cells to facilitate myelin debris clearance and accelerate nerve repairment after spinal cord injury. Acta

pharmacologica Sinica. 2022;43(6):1360-71.https://doi.org/10.1038/s41401-021-00759-5

14. Yuan J, Amin P, Ofengeim D. Necroptosis and RIPK1-mediated neuroinflammation in CNS diseases. Nature reviews Neuroscience. 2019;20(1):19-33.https://doi.org/10.1038/s41583-018-0093-1
15. Liu M Fau - Wu W, Wu W Fau - Li H, Li H Fau - Li S, Li S Fau - Huang L-t, Huang Lt Fau - Yang Y-q, Yang Yq Fau - Sun Q, et al. Necroptosis, a novel type of programmed cell death, contributes to early neural cells damage after spinal cord injury in adult mice. (2045-7723 (Electronic)).
16. Liu S, Li Y, Choi HMC, Sarkar C, Koh EY, Wu J, et al. Lysosomal damage after spinal cord injury causes accumulation of RIPK1 and RIPK3 proteins and potentiation of necroptosis. Cell death & disease. 2018;9(5):476.https://doi.org/10.1038/s41419-018-0469-1
17. Wang F, Gómez-Sintes R, Boya P. Lysosomal membrane permeabilization and cell death. Traffic (Copenhagen, Denmark). 2018;19(12):918-31.https://doi.org/10.1111/tra.12613
18. Boya P, Kroemer G. Lysosomal membrane permeabilization in cell death. Oncogene. 2008;27(50):6434-51.https://doi.org/10.1038/onc.2008.310
19. Lee JC, Simonyi A, Sun AY, Sun GY. Phospholipases A2 and neural membrane dynamics: implications for Alzheimer's disease. Journal of neurochemistry. 2011;116(5):813-9.https://doi.org/10.1111/j.1471-4159.2010.07033.x
20. Li Y, Jones JW, H MCC, Sarkar C, Kane MA, Koh EY, et al. cPLA2 activation contributes to lysosomal defects leading to impairment of autophagy after spinal cord injury. Cell death & disease. 2019;10(7):531.https://doi.org/10.1038/s41419-019-1764-1
21. Zhang H, Yin Y, Liu Y, Zou G, Huang H, Qian P, et al. Necroptosis mediated by impaired autophagy flux contributes to adverse ventricular remodeling after myocardial infarction. (1873-2968 (Electronic)).
22. Xu Y, Hu X, Li F, Zhang H, Lou J, Wang X, et al. GDF-11 Protects the Traumatically Injured Spinal Cord by Suppressing Pyroptosis and Necroptosis via TFE3-Mediated Autophagy Augmentation. (1942-0994 (Electronic)).
23. Staples M, Acosta S, Tajiri N, Pabon M, Kaneko Y, Borlongan CV. Delta opioid receptor and its peptide: a receptor-ligand neuroprotection. International journal of molecular sciences. 2013;14(9):17410-9.https://doi.org/10.3390/ijms140917410
24. Klenowski P, Morgan M, Bartlett SE. The role of δ-opioid receptors in learning and memory underlying the development of addiction. British journal of pharmacology. 2015;172(2):297-310.https://doi.org/10.1111/bph.12618
25. Pradhan AA, Befort K, Nozaki C, Gavériaux-Ruff C, Kieffer BL. The delta opioid receptor: an evolving target for the treatment of brain disorders. Trends in pharmacological sciences. 2011;32(10):581-90.https://doi.org/10.1016/j.tips.2011.06.008
26. He X, Sandhu HK, Yang Y, Hua F, Belser N, Kim DH, et al. Neuroprotection against hypoxia/ischemia: δ-opioid receptor-mediated cellular/molecular events. Cellular and molecular life sciences : CMLS. 2013;70(13):2291-303.https://doi.org/10.1007/s00018-012-1167-2
27. Husain S, Ahmad A, Singh S, Peterseim C, Abdul Y, Nutaitis MJ. PI3K/Akt Pathway: A Role in δ-Opioid Receptor-Mediated RGC Neuroprotection. Investigative ophthalmology & visual science.

2017;58(14):6489-99.https://doi.org/10.1167/iovs.16-20673

28. Wang S, Cao X, Duan YA-O, Zhang G. Delta Opioid Peptide [d-Ala2, d-Leu5] Enkephalin (DADLE) Exerts a Cytoprotective Effect in Astrocytes Exposed to Oxygen-Glucose Deprivation by Inducing Autophagy. (1555-3892 (Electronic)).
29. Lai Z, Gu L, Yu L, Chen H, Yu Z, Zhang C, et al. Delta opioid peptide [d-Ala2, d-Leu5] enkephalin confers neuroprotection by activating delta opioid receptor-AMPK-autophagy axis against global ischemia. (2045-3701 (Print)).
30. Guo R, Chen P, Fu T, Zhang R, Zhu Y, Jin N, et al. Activation of Delta-Opioid Receptor Protects ARPE19 Cells against Oxygen-Glucose Deprivation/Reoxygenation-Induced Necroptosis and Apoptosis by Inhibiting the Release of TNF-α. (2090-004X (Print)).
31. Lilley E, Andrews MR, Bradbury EJ, Elliott H, Hawkins P, Ichiyama RM, et al. Refining rodent models of spinal cord injury. (1090-2430 (Electronic)).
32. Nguyen TTT, Ishida CT, Shang E, Shu C, Torrini C, Zhang Y, et al. Activation of LXRβ inhibits tumor respiration and is synthetically lethal with Bcl-xL inhibition. (1757-4684 (Electronic)).
33. Tu YA-O, Jiang ST, Chiang CW, Chen LC, Huang CC. Endothelial-specific insulin receptor substrate-1 overexpression worsens neonatal hypoxic-ischemic brain injury via mTOR-mediated tight junction disassembly. (2058-7716 (Print)).
34. Iwata M, Inoue S Fau - Kawaguchi M, Kawaguchi M Fau - Nakamura M, Nakamura M Fau - Konishi N, Konishi N Fau - Furuya H, Furuya H. Effects of delta-opioid receptor stimulation and inhibition on hippocampal survival in a rat model of forebrain ischaemia. (0007-0912 (Print)).
35. Zhang H, Ni W, Yu G, Geng Y, Lou J, Qi J, et al. 3,4-Dimethoxychalcone, a caloric restriction mimetic, enhances TFEB-mediated autophagy and alleviates pyroptosis and necroptosis after spinal cord injury. (1838-7640 (Electronic)).
36. Hu J, Han H, Cao P, Yu W, Yang C, Gao Y, et al. Resveratrol improves neuron protection and functional recovery through enhancement of autophagy after spinal cord injury in mice. (1943-8141 (Print)).
37. Zhou Y, Zhou B, Pache L, Chang MA-OX, Khodabakhshi AH, Tanaseichuk O, et al. Metascape provides a biologist-oriented resource for the analysis of systems-level datasets. (2041-1723 (Electronic)).
38. Stavoe AKH, Holzbaur ELF. Autophagy in Neurons. (1530-8995 (Electronic)).
39. Ray SK. Modulation of autophagy for neuroprotection and functional recovery in traumatic spinal cord injury. (1673-5374 (Print)).
40. Wu C, Chen H, Zhuang R, Zhang H, Wang Y, Hu X, et al. Betulinic acid inhibits pyroptosis in spinal cord injury by augmenting autophagy via the AMPK-mTOR-TFEB signaling pathway. (1449-2288 (Electronic)).
41. Glick D, Barth S, Macleod KF. Autophagy: cellular and molecular mechanisms. The Journal of pathology. 2010;221(1):3-12.https://doi.org/10.1002/path.2697
42. !!! INVALID CITATION !!! .

43. Fricker M, Tolkovsky AM, Borutaite V, Coleman M, Brown GC. Neuronal Cell Death. (1522-1210 (Electronic)).
44. Mauthe M, Orhon I, Rocchi C, Zhou X, Luhr M, Hijlkema KJ, et al. Chloroquine inhibits autophagic flux by decreasing autophagosome-lysosome fusion. (1554-8635 (Electronic)).
45. Sarkar C, Jones JW, Hegdekar N, Thayer JA, Kumar A, Faden AI, et al. PLA2G4A/cPLA2-mediated lysosomal membrane damage leads to inhibition of autophagy and neurodegeneration after brain trauma. Autophagy. 2020;16(3):466-85.https://doi.org/10.1080/15548627.2019.1628538
46. Gao K, Niu J, Dang X. Neuroprotection of melatonin on spinal cord injury by activating autophagy and inhibiting apoptosis via SIRT1/AMPK signaling pathway. Biotechnology letters. 2020;42(10):2059-69.https://doi.org/10.1007/s10529-020-02939-5
47. Guo R, Gao S, Feng Y, Mao C, Sheng W. Ulinastatin attenuates spinal cord injury by targeting AMPK/NLRP3 signaling pathway. Journal of chemical neuroanatomy. 2022;125:102145.https://doi.org/10.1016/j.jchemneu.2022.102145
48. Wu C, Chen H, Zhuang R, Zhang H, Wang Y, Hu X, et al. Betulinic acid inhibits pyroptosis in spinal cord injury by augmenting autophagy via the AMPK-mTOR-TFEB signaling pathway. International journal of biological sciences. 2021;17(4):1138-52.https://doi.org/10.7150/ijbs.57825
49. Wang C, Wang Q, Lou Y, Xu J, Feng Z, Chen Y, et al. Salidroside attenuates neuroinflammation and improves functional recovery after spinal cord injury through microglia polarization regulation. Journal of cellular and molecular medicine. 2018;22(2):1148-66.https://doi.org/10.1111/jcmm.13368
50. Lin LL, Wartmann M, Lin AY, Knopf JL, Seth A, Davis RJ. cPLA2 is phosphorylated and activated by MAP kinase. Cell. 1993;72(2):269-78.https://doi.org/10.1016/0092-8674(93)90666-e
51. Ke S, Dian-san S Fau - Xiang-rui W, Xiang-rui W. Delta opioid agonist [D-Ala2, D-Leu5] enkephalin (DADLE) reduced oxygen-glucose deprivation caused neuronal injury through the MAPK pathway. (1872-6240 (Electronic)).
52. Beal EW, Kim JL, Reader BF, Akateh C, Maynard K, Washburn WK, et al. [D-Ala(2), D-Leu(5)] Enkephalin Improves Liver Preservation During Normothermic Ex Vivo Perfusion. (1095-8673 (Electronic)).
53. Fu D, Liu H, Liu H, Yao J. Effects of D-Ala2, D-Leu5-Enkephalin pre- and post-conditioning in a rabbit model of spinal cord ischemia and reperfusion injury. (1791-3004 (Electronic)).
54. Liao HY, Wang ZQ, Ran R, Zhou KS, Ma CW, Zhang HH. Biological Functions and Therapeutic Potential of Autophagy in Spinal Cord Injury. Frontiers in cell and developmental biology. 2021;9:761273.https://doi.org/10.3389/fcell.2021.761273
55. Parzych KR, Klionsky DJ. An overview of autophagy: morphology, mechanism, and regulation. (1557-7716 (Electronic)).
56. Kanno H, Ozawa H, Sekiguchi A, Itoi E. The role of autophagy in spinal cord injury. Autophagy. 2009;5(3):390-2.https://doi.org/10.4161/auto.5.3.7724

57. Fan H, Tang HB, Shan LQ, Liu SC, Huang DG, Chen X, et al. Quercetin prevents necroptosis of oligodendrocytes by inhibiting macrophages/microglia polarization to M1 phenotype after spinal cord injury in rats. Journal of neuroinflammation. 2019;16(1):206.https://doi.org/10.1186/s12974-019-1613-2
58. Yuan J, Amin P, Ofengeim D. Necroptosis and RIPK1-mediated neuroinflammation in CNS diseases. (1471-0048 (Electronic)).
59. Sugaya TA-O, Kanno HA-O, Matsuda M, Handa KA-O, Tateda S, Murakami T, et al. B-RAF(V600E) Inhibitor Dabrafenib Attenuates RIPK3-Mediated Necroptosis and Promotes Functional Recovery after Spinal Cord Injury. LID - 10.3390/cells8121582 [doi] LID - 1582. (2073-4409 (Electronic)).
60. Liang YX, Wang NN, Zhang ZY, Juan ZD, Zhang C. Necrostatin-1 Ameliorates Peripheral Nerve Injury-Induced Neuropathic Pain by Inhibiting the RIP1/RIP3 Pathway. (1662-5102 (Print)).
61. Aits S, Kricker J Fau - Liu B, Liu B Fau - Ellegaard A-M, Ellegaard Am Fau - Hämälistö S, Hämälistö S Fau - Tvingsholm S, Tvingsholm S Fau - Corcelle-Termeau E, et al. Sensitive detection of lysosomal membrane permeabilization by lysosomal galectin puncta assay. (1554-8635 (Electronic)).
62. Kim Yc Fau - Guan K-L, Guan KL. mTOR: a pharmacologic target for autophagy regulation. (1558-8238 (Electronic)).
63. Kim J, Kundu M Fau - Viollet B, Viollet B Fau - Guan K-L, Guan KL. AMPK and mTOR regulate autophagy through direct phosphorylation of Ulk1. (1476-4679 (Electronic)).
64. Mihaylova MM, Shaw RJ. The AMPK signalling pathway coordinates cell growth, autophagy and metabolism. (1476-4679 (Electronic)).
65. Husted TL, Govindaswami M Fau - Oeltgen PR, Oeltgen Pr Fau - Rudich SM, Rudich Sm Fau - Lentsch AB, Lentsch AB. A delta2-opioid agonist inhibits p38 MAPK and suppresses activation of murine macrophages. (0022-4804 (Print)).
66. Bae EJ, Lee HJ, Jang YH, Michael S, Masliah E, Min DS, et al. Phospholipase D1 regulates autophagic flux and clearance of α-synuclein aggregates. (1476-5403 (Electronic)).
67. Hartz AMS, Rempe RG, Soldner ELB, Pekcec A, Schlichtiger J, Kryscio R, et al. Cytosolic phospholipase A2 is a key regulator of blood-brain barrier function in epilepsy. (1530-6860 (Electronic)).
68. Zhou LA-O, Zhou L, Su LA-O, Cao SL, Xie YA-O, Wang N, et al. Celecoxib Ameliorates Seizure Susceptibility in Autosomal Dominant Lateral Temporal Epilepsy. (1529-2401 (Electronic)).
69. Jin W, Zhao J, Yang E, Wang Y, Wang Q, Wu Y, et al. Neuronal STAT3/HIF-1α/PTRF axis-mediated bioenergetic disturbance exacerbates cerebral ischemia-reperfusion injury via PLA2G4A. (1838-7640 (Electronic)).
70. Zheng L, Xie C, Zheng J, Dong Q, Si T, Zhang J, et al. An imbalanced ratio between PC(16:0/16:0) and LPC(16:0) revealed by lipidomics supports the role of the Lands cycle in ischemic brain injury. (1083-351X (Electronic)).

Figures

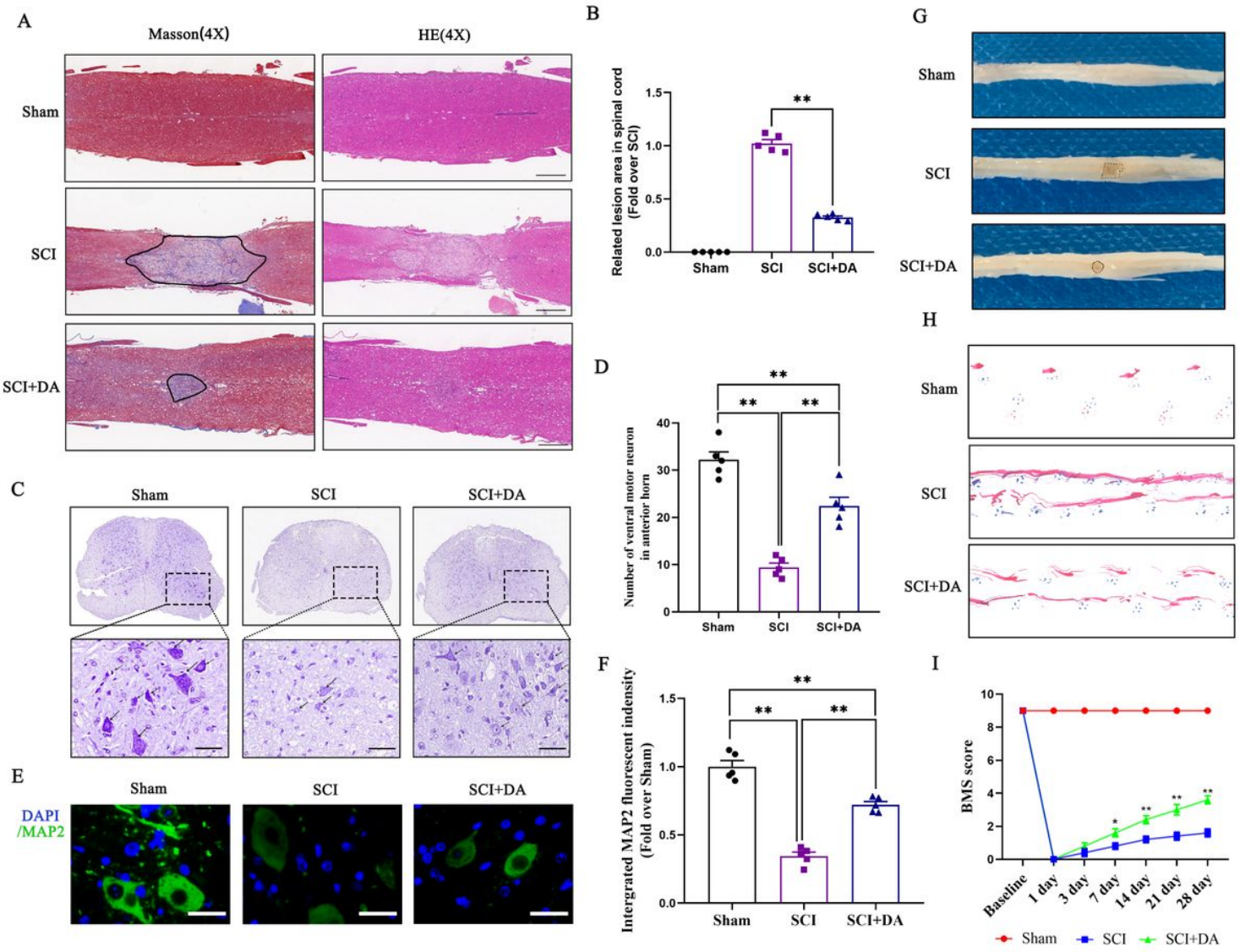

Figure 1

DADLE promotes mice locomotive function recovery after SCI.(A) Longitudinal spinal cord sections from the sham, SCI and SCI+DA groups at 28 days were examined via HE dyeing and Masson dyeing (scale bar = 400 μm). (B) Quantitative investigations of Masson-positive lesions within the spinal cord of the respective groups. (C) Cross section of mice spinal cord from respective groups at 28 days were examined via Nissl dyeing. The overview of the spinal cord was observed at 4X and anterior horn of spinal cord was observed at 20X (scale bar=50μm). The black arrow indicates the neuron. (D) Counting analysis of ventricle motor neurons in the cross section of spinal cord from respective groups. (E) Photographs of spinal cord sections in the respective groups stained with antibody MAP2 (green) (scale bar = 25 μm). (F) Quantification of MAP2 optical density within a spinal cord in each group. (G) Photographs of spinal cord section on mice in sham, SCI and SCI+DA groups at 28 days after surgery. (H)

Photographs of mouse footprints in each group following 28 days. Blue: forepaw print; Red: hind paw print. (I) Basso mouse scale (BMS) for the indicated groups at days 0, 1, 3, 7, 14, 21, and 28. The data are shown as the mean ± SEM. n = 5. *P < 0.05, **P < 0.01. ns indicates no significance.

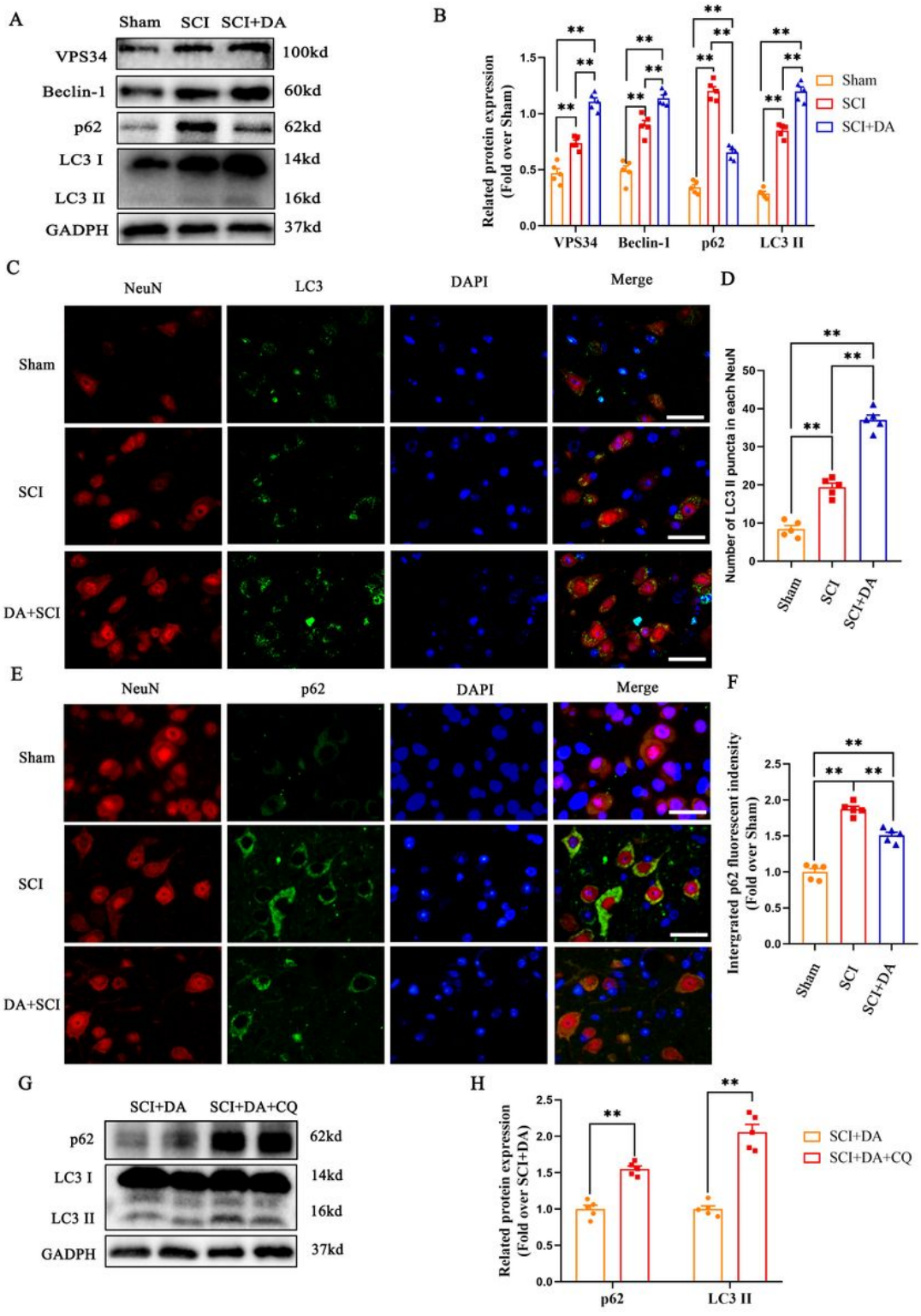

Figure 2

DADLE promotes autophagic flux after SCI. (A)Western blotting to assess VPS34, beclin-1, p62 and LC3 expression levels in the Sham, SCI, and SCI+DA groups. GAPDH was utilized as a loading control. (B) The quantification of VPS34, beclin-1, p62 and LC3-II expression levels were analyzed in each group. (C) Double immunofluorescence staining of LC3(green) and NeuN (red) in the spinal cords of the Sham, SCI, and SCI+DA groups (scale bar= 25μm) (D) Number of LC3 II puncta in each neuron on the right. (E) Double immunofluorescence staining of p62 (green) and NeuN (red) in the spinal cords of the Sham, SCI, and SCI+DA groups (scale bar= 25μm) (F) Quantified related p62 immunofluorescent density data in each group are presented on the right. (G) Western blotting for P62 and LC3 II expression levels in SCI+DA and SCI+DA+CQ groups to assess autophagic flux. (H) Quantification of p62 and LC3-II expression levels were analyzed in SCI+DA and SCI+DA+CQ groups.GAPDH was utilized as a loading control. The data are shown as the mean ± SEM. N = 5. *P < 0.05, **P < 0.01. ns indicates no significance.

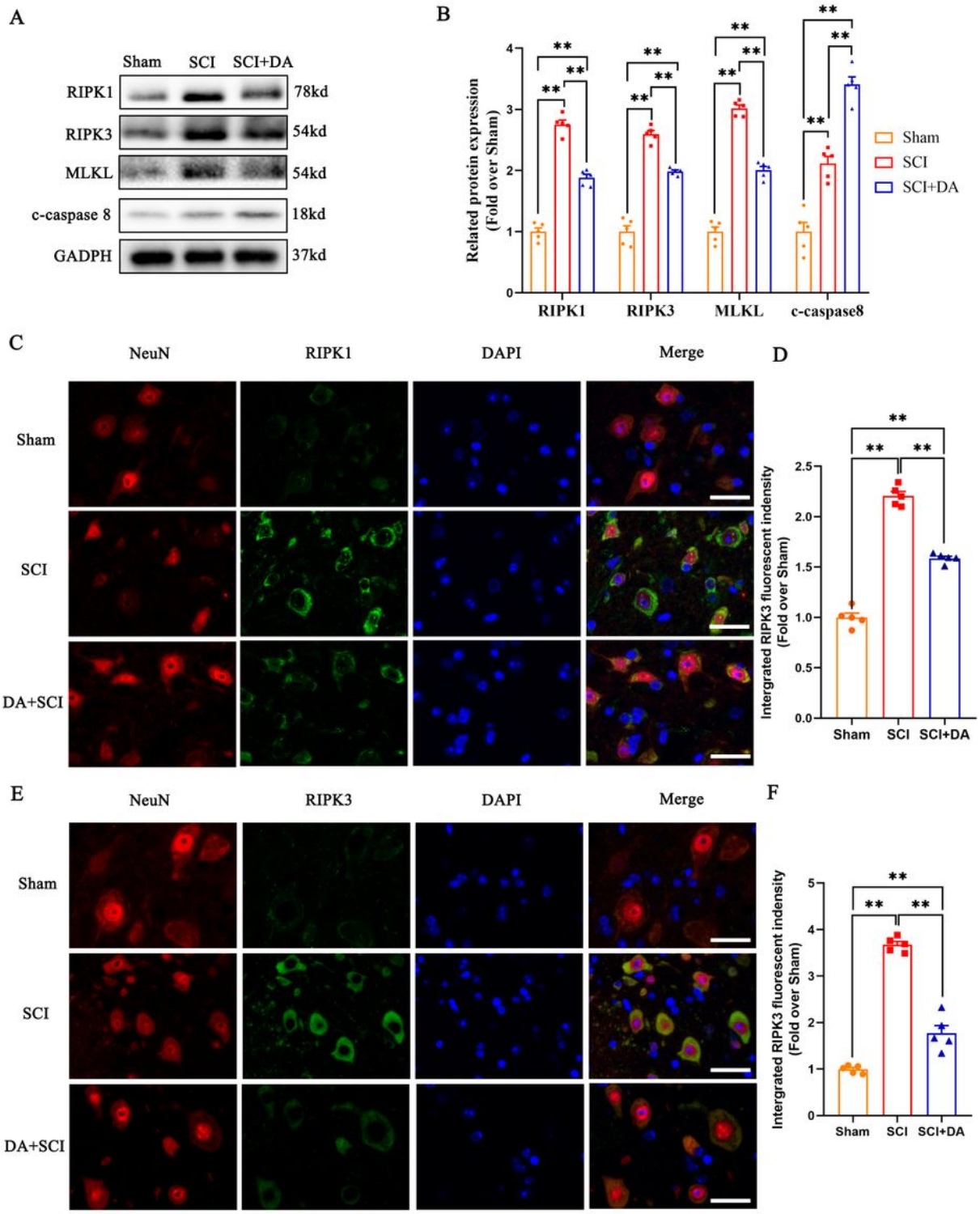

Figure 3

DADLE inhibits necroptosis after SCI. (A) Western blotting for RIPK1, RIPK3, MLKL and c-caspase-8 expression levels in the Sham, SCI, and SCI+DA groups. GAPDH was utilized as a loading control. (B) The quantification of the RIPK1, RIPK3, MLKL and c-caspase-8 expression levels were analyzed in each group. (C) Double immunofluorescence staining of RIPK1 (green) and NeuN (red) in the spinal cords of the Sham, SCI, and SCI+DA groups (scale bar= 25μm) (D) Quantified immunofluorescent density data of

RIPK1 are presented on the right. (E) Double immunofluorescence staining of RIPK3 (green) and NeuN (red) in the spinal cords of the Sham, SCI, and SCI+DA groups (scale bar= 25μm) (F) Quantified immunofluorescent density data of RIPK3 are presented on the right. The data are shown as the mean ± SEM. n = 5. *P < 0.05, **P < 0.01. ns indicates no significance.

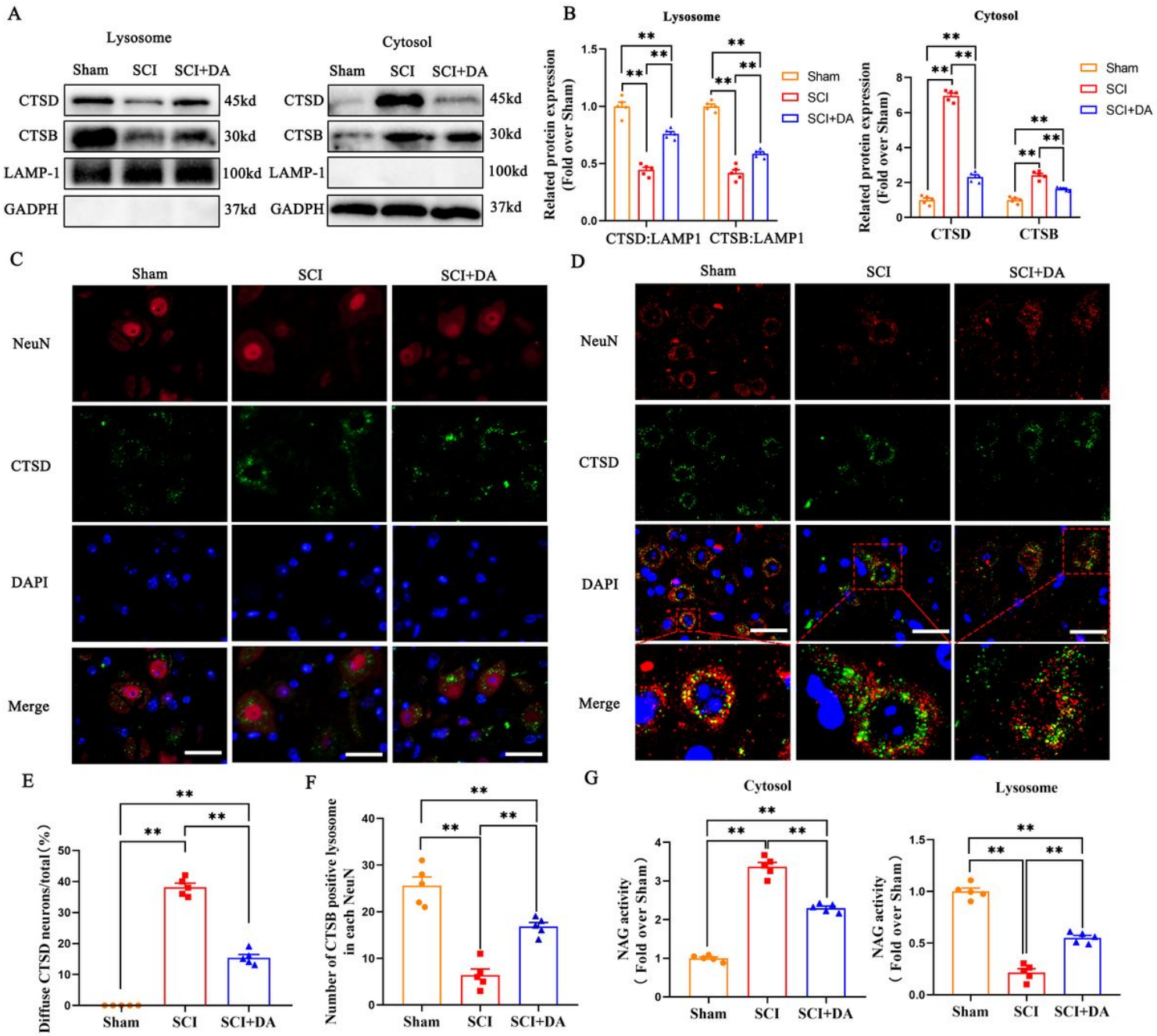

Figure 4

DADLE inhibits lysosomal membrane permeabilization after SCI.(A) Western blotting for CTSB, CTSD and LAMP1 expression levels in the cytoplasm and lysosomes extracted from the spinal cord of Sham, SCI, SCI+DA groups. Lysosomal membrane protein LAMP1 was utilized as a loading control in lysosomal fraction. GAPDH was utilized as a loading control in cytosol fraction. (B) Quantification of the protein

levels of CTSB and CTSD in the cytoplasm and lysosomes extracted from the spinal cord. (C) Immunofluorescence staining of CTSD (green) and NeuN (red) in the spinal cord from Sham, SCI, and SCI+DA groups on postoperative day 3 (scale bar= 25μm). (D) Immunofluorescence staining of CTSD (green) and LAMP1 (red) in the spinal cord from Sham, SCI and SCI+DA groups. LAMP1 was used to visualize lysosome. (E) Comparison of the ratio of diffuse CTSD neuron in the anterior horn of spinal cord from Sham, SCI and SCI+DA groups. (F) Positive CTSB lysosome in each neuron from the date of (D). (G) Date of enzyme activity of NAG in the lysosome or cytosol extracted from spinal cord from Sham, SCI and SCI+DA groups. The data are shown as the mean ± SEM. n = 5. *P < 0.05, **P < 0.01. ns indicates no significance.

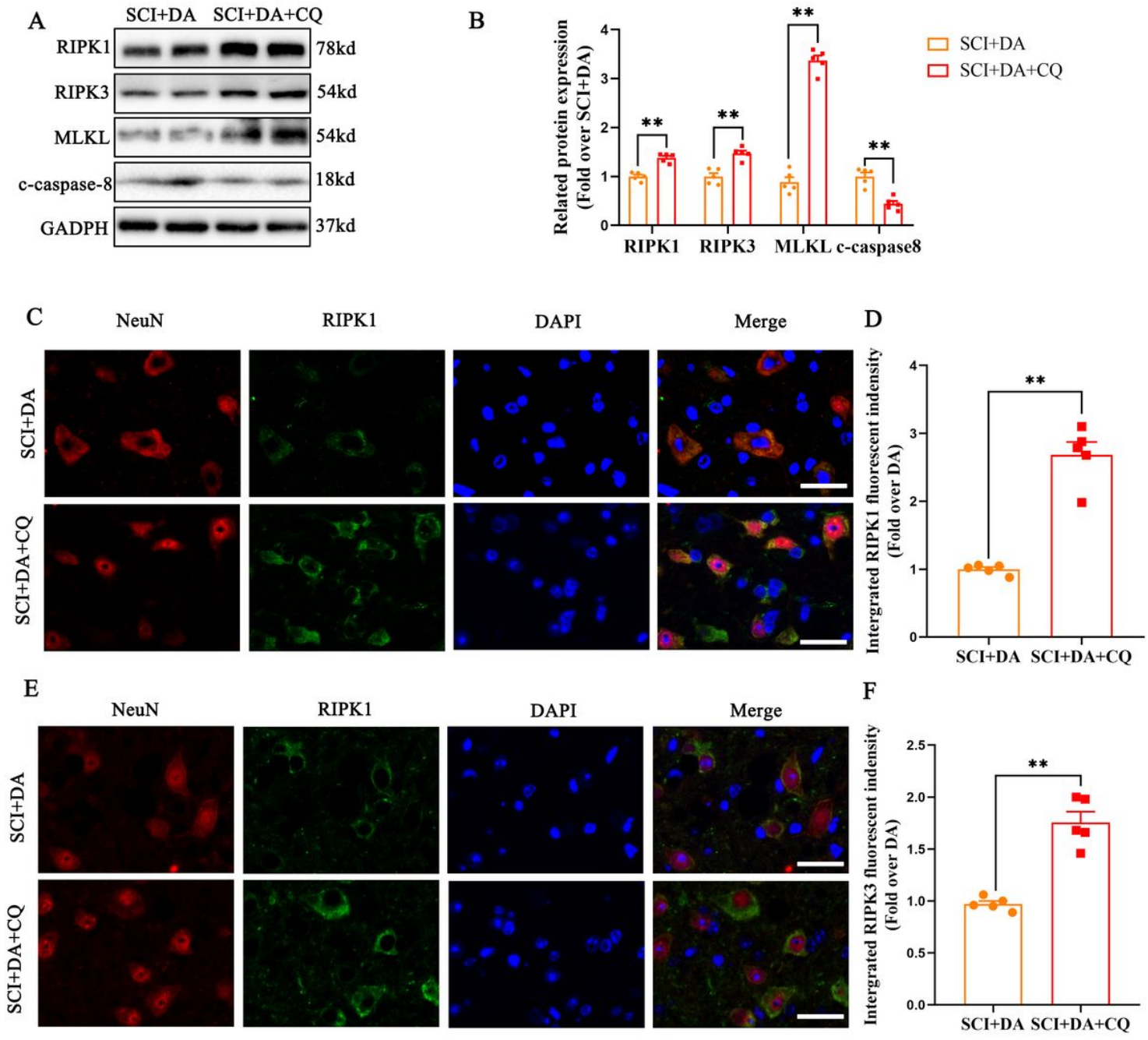

Figure 5

Blockage of autophagic flux by CQ weakens inhibitory effect of DADLE on necroptosis in SCI. (A) WB analyses of expression levels of RIPK1, RIPK3, MLKL and c-caspase-8 in the injured spinal cord lesion. GAPDH was utilized as a loading control. (B) The analysis of RIPK1, RIPK3, MLKL and c-caspase-8 expression levels were quantified in each group. (C) Double immunofluorescence staining of RIPK1 (green) and NeuN (red) in the spinal cords of the DADLE and DADLE+CQ groups (scale bar= 25μm). (D) Quantified immunofluorescent density data of RIPK1 are presented on the right. (E) Double

immunofluorescence staining of RIPK3 (green) and NeuN (red) in the spinal cords of the SCI+DA and SCI+DA+CQ groups (scale bar= 25μm). (F) Quantified immunofluorescent density data of RIPK3 are presented on the right. The data are shown as the mean ± SEM. n = 5. *P < 0.05, **P < 0.01. ns indicates no significance.

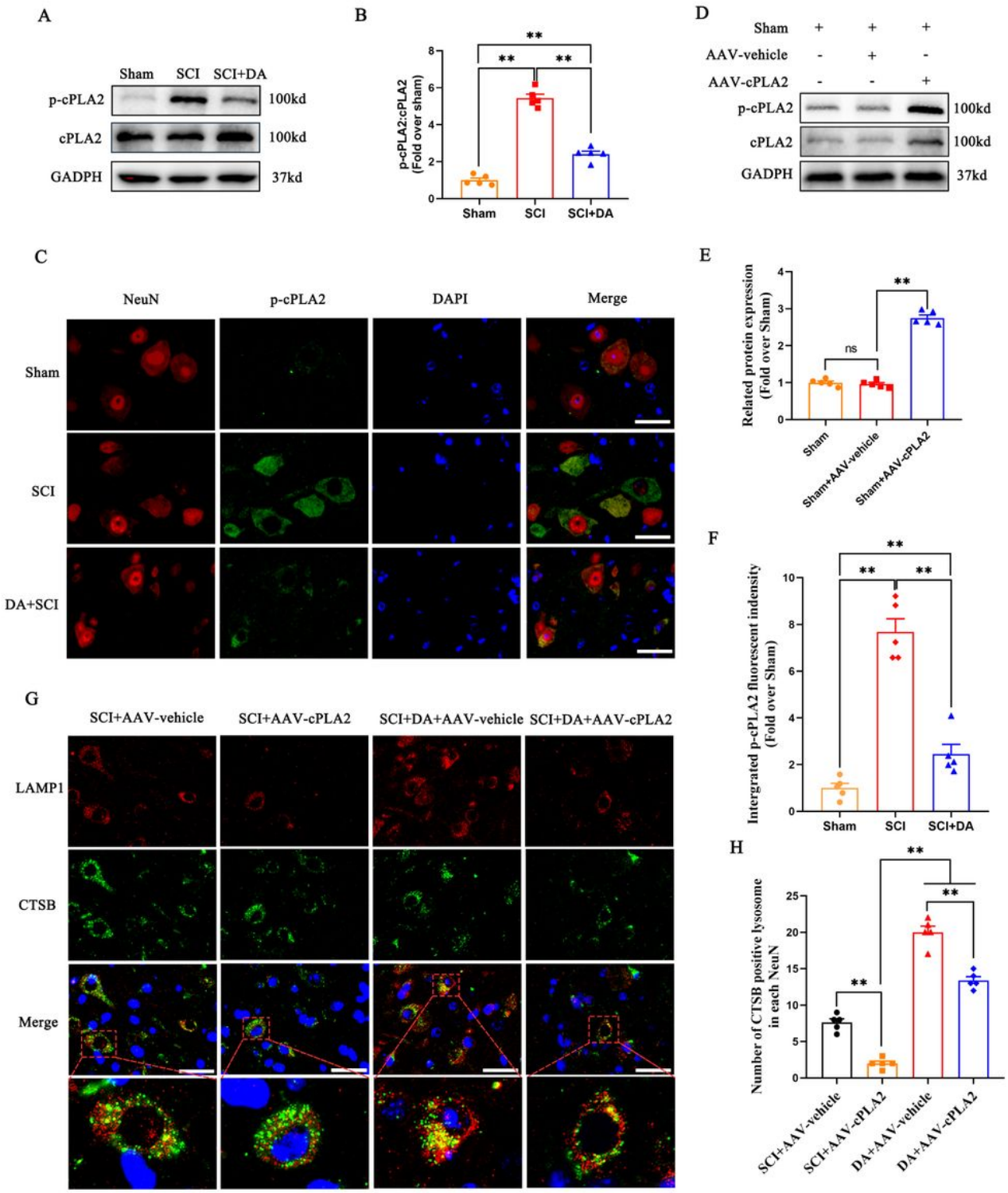

Figure 6

DADLE inhibits LMP by decreasing cPLA2 phosphorylation following SCI (A)cPLA2 and p-cPLA2 protein levels in the spinal cord from three groups on postoperative day 3. GAPDH was utilized as a loading control. (B) Quantification of the protein expression levels of p-cPLA2/cPLA2 in the spinal cord. (C) Immunofluorescence staining of NeuN (red) and p-cPLA2 (green) in the anterior horn of spinal cord from three groups on postoperative day 3. (scale bar= 25μm). (D) Western blotting for protein expression levels of cPLA2 and p-cPLA2 from the spinal cord of Sham, Sham+AAV-vhicle and Sham +AAV-cPLA2. GAPDH was utilized as a loading control. (E) Quantification of the protein expression levels of p-cPLA2 and cPLA2 in the spinal cord from the result of (D). (F) Quantified immunofluorescent density data of p-cPLA2 are presented on the right (G) Immunofluorescence staining of CTSB (green) and LAMP1 (red) in the spinal cord from SCI+AAV-vhicle, SCI+AAV-cPLA2, SCI+DA+ AAV-vhicle and SCI+DA+AAV-cPLA2 groups. LAMP1 was used to visualize lysosome. (H) Positive CTSB lysosome in each neuron from the date of (G). The data are shown as the mean ± SEM. n = 5. *P < 0.05, **P < 0.01. ns indicates no significance.

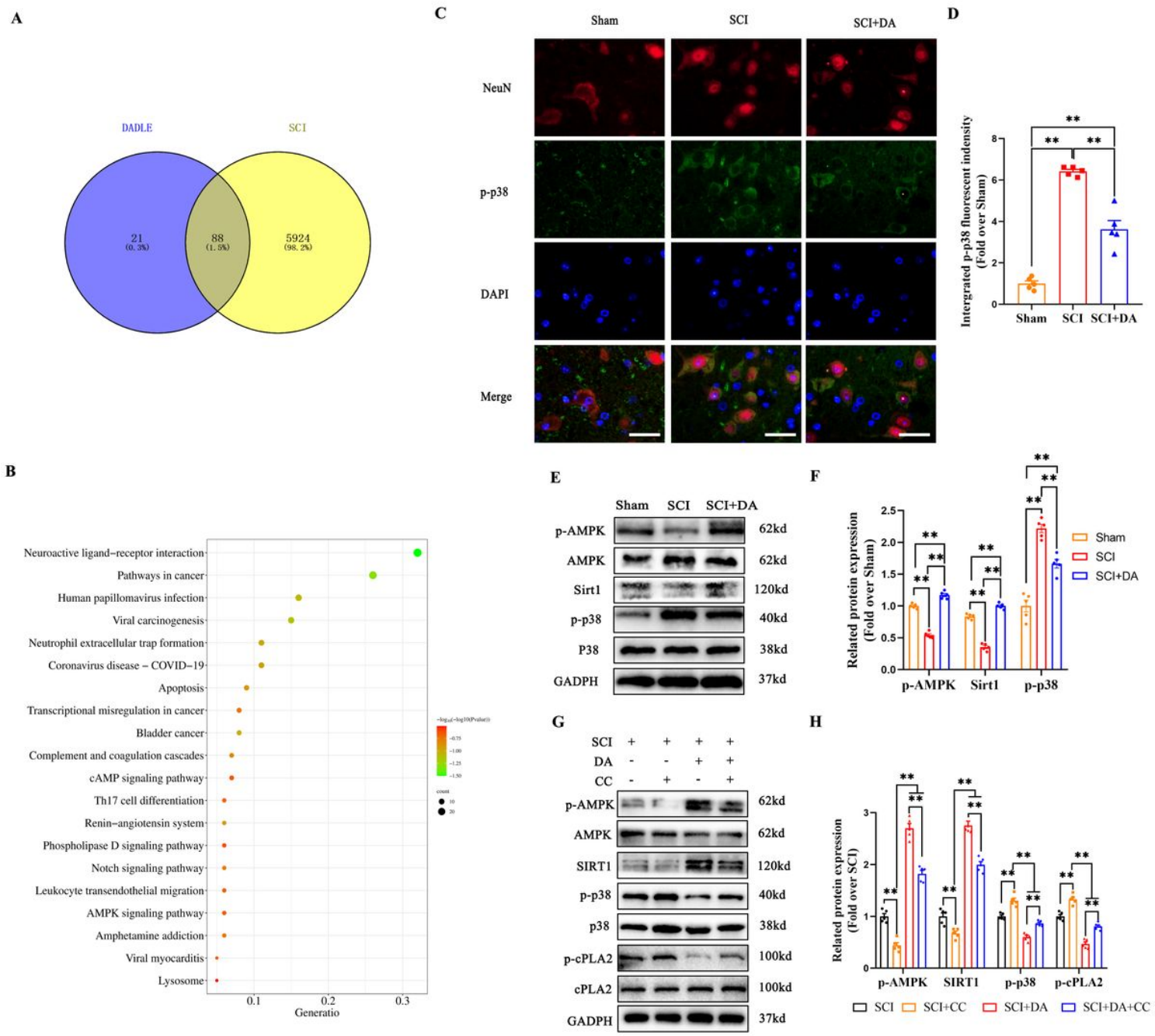

Figure 7

DADLE promotes autophagy and inhibits necroptosis through DOR-AMPK-SIRT1-P38 pathwayin SCI (A) Venn diagram showing the overlapping gene by SCI target gene and DADLE predicted target gene. (B) The top 15 enriched KEGG pathways of the overlapping gene of (A). (C) Double immunofluorescence staining of p-p38 (green) and NeuN (red) in the spinal cords of the Sham, SCI and SCI+DA groups (scale bar= 25μm). (D) Quantified immunofluorescent density data of p-p38 are presented on the right (E) Western blotting for protein expression levels of AMPK, p-AMPK, SIRT1, p38, p-p38 from the spinal cord of

Sham, SCI and SCI+DA groups, GAPDH was utilized as a loading control. (F) Quantification of the related protein expression levels of p-AMPK, SIRT1 and p-p38 in the spinal cord from the result of (D). (G) Western blotting for protein expression levels of AMPK, p-AMPK, SIRT1, p38, p-p38 from the spinal cord of SCI, SCI+CC, SCI+DA and SCI+DA+CC groups, GAPDH was utilized as a loading control. (H) Quantification of the related protein expression levels of AMPK, SIRT1 and p-p38 in the spinal cord from the result of (G). The data are shown as the mean ± SEM. n = 5. *P < 0.05, **P < 0.01. ns indicates no significance.

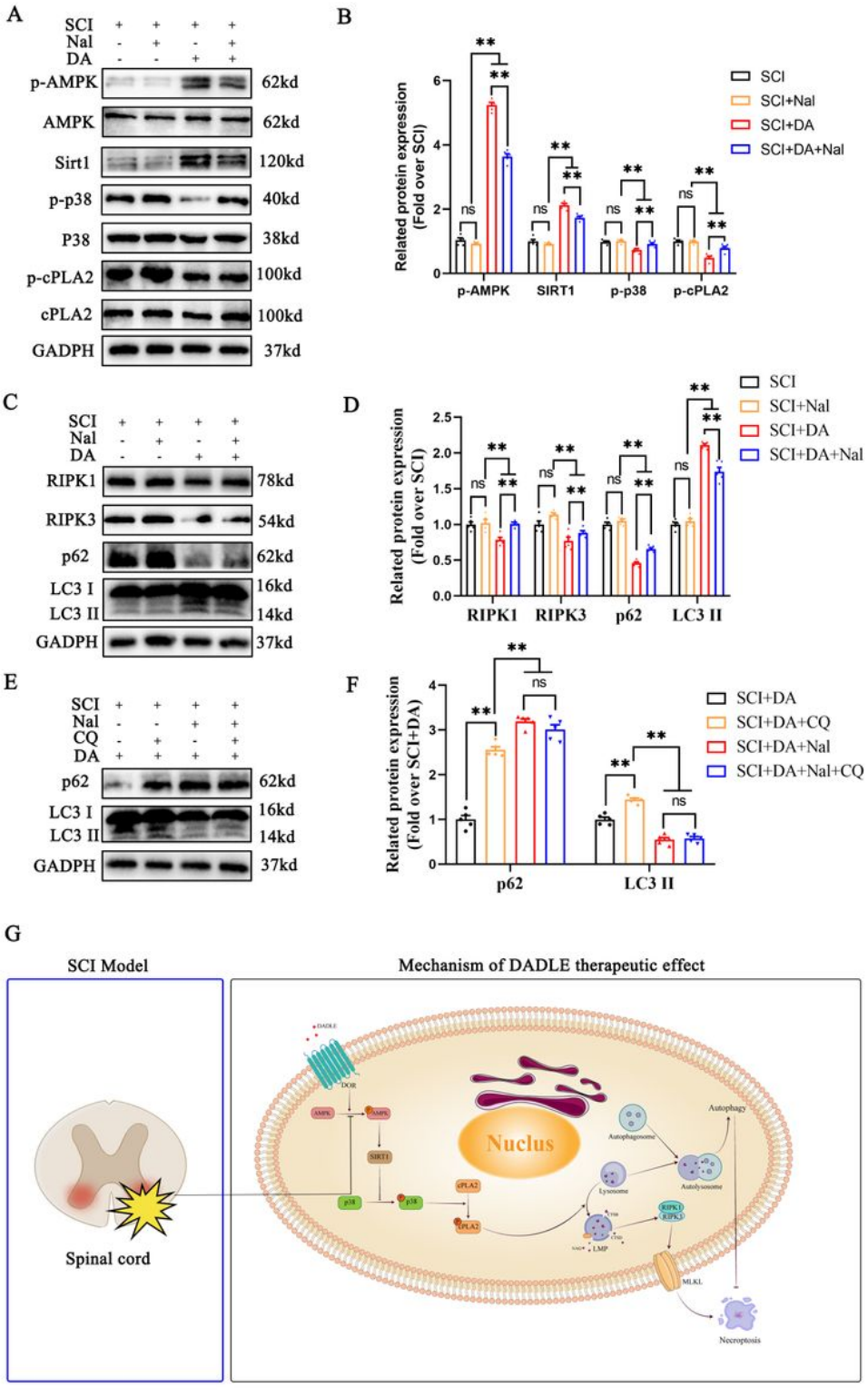

Figure 8

Inhibition of DOR-AMPK-SIRT1-P38 pathway reverses neural protective effect by DADLE after SCI (A) Western blotting for protein expression levels of AMPK, p-AMPK, SIRT1, p38, p-p38, cPLA2 and p-cPLA2 from the spinal cord of SCI, SCI+Nal, SCI+DA, SCI+DA+Nal groups. GAPDH was utilized as a loading control. (B) The analysis of p-AMPK, SIRT1, p-p38 and p-cPLA2 expression levels were quantified in each group. (C) Western blotting for protein expression levels of RIPK1, RIPK3, p62 and LC3 from the spinal cord of SCI, SCI+Nal, SCI+DA, SCI+DA+Nal groups. GAPDH was utilized as a loading control. (D) The analysis of RIPK1, RIPK3, p62 and LC3II expression levels were quantified in each group. (E) Western blotting for protein expression levels of p62 and LC3 from the spinal cord of SCI+DA, SCI+DA+CQ, SCI+DA+Nal and SCI+DA+Nal+CQ groups. GAPDH was utilized as a loading control. (F) The analysis of p62 and LC3II expression levels were quantified in each group from the result of (E). (G) Schematic diagram showing the potential protective effect of DADLE against SCI. The data are shown as the mean ± SEM. n = 5. *P < 0.05, **P < 0.01. ns indicates no significance.

Supplementary Files

This is a list of supplementary files associated with this preprint. Click to download.

- FigureS1.jpg
- FigureS2.jpg
- FigureS3.jpg